AFRL-VS-HA-TR-2005-1031

ANALYSIS AND SIMULATION OF CAVITY-DECOUPLED CHEMICAL EXPLOSIONS

Jeffry L. Stevens
Norton Rimer
Hemig Xu
John R. Murphy
Brian W. Barker
Evan Bailey
Steven J. Gibbons
Conrad Lindholm
Frode Ringdal
Tormod Kvaerna
Ivan Kitov

Science Applications International Corporation
10260 Campus Point Drive
San Diego, CA 92121-1578

22 December 2004

Final Report

AIR FORCE RESEARCH LABORATORY
Space Vehicles Directorate
29 Randolph Rd
AIR FORCE MATERIEL COMMAND
Hanscom AFB, MA 01731-3010

This technical report has been reviewed and is approved for publication.

AFRL-VS-HA-TR-2005-1031

/signed/

ROBERT J. RAISTRICK
Contract Manager

/signed/

ROBERT BELAND, Chief
Battlespace Surveillance Innovation Center

This report has been reviewed by the ESC Public Affairs Office (PA) and is releasable to the National Technical Information Service (NTIS).

Qualified requestors may obtain additional copies from the Defense Technical Information Center (DTIC). All others should apply to the National Technical Information Service.

If your address has changed, if you wish to be removed from the mailing list, or if the addressee is no longer employed by your organization, please notify AFRL/VSIM, 29 Randolph Rd., Hanscom AFB, MA 01731-3010. This will assist us in maintaining a current mailing list.

Do not return copies of this report unless contractual obligations or notices on a specific document require that it be returned.

Using Government drawings, specifications, or other data included in this document for any purpose other than Government procurement does not in any way obligate the U.S. Government. The fact that the Government formulated or supplied the drawings, specifications, or other data does not license the holder or any other person or corporation; or convey any rights or permission to manufacture, use, or sell any patented invention that may relate to them.

REPORT DOCUMENTATION PAGE

Form Approved
OMB No. 0704-0188

1. REPORT DATE *(DD-MM-YYYY)*	2. REPORT TYPE	3. DATES COVERED *(From - To)*
22-12-2004	Final	20 Sep 2001 to 19 Dec 2004

4. TITLE AND SUBTITLE
Analysis and Simulation of Cavity-Decoupled Chemical Explosions

5a. CONTRACT NUMBER
DTRA01-01-C-0069

5b. GRANT NUMBER

5c. PROGRAM ELEMENT NUMBER

6. AUTHOR(S)
Jeffry L. Stevens*, Norton Rimer*, Heming Xu*, John R. Murphy*, Brian W. Barker*, Evan Bailey*, Steven J. Gibbons**, Conrad Lindholm**, Frode Ringdal**, Tormod Kvaerna**, Ivan Kitov***

5d. PROJECT NUMBER
DTRA

5e. TASK NUMBER
OT

5f. WORK UNIT NUMBER
A1

7. PERFORMING ORGANIZATION NAME(S) AND ADDRESS(ES)

Science Applications International Corporation
10260 Campus Point Drive
San Diego, CA 92121-1578

8. PERFORMING ORGANIZATION REPORT NUMBER

9. SPONSORING / MONITORING AGENCY NAME(S) AND ADDRESS(ES)
Air Force Research Laboratory
29 Randolph Road
Hanscom AFB, MA 01731-3010

Contract Manager: R. Raistrick AFRL/VSBYE

10. SPONSOR/MONITOR'S ACRONYM(S)
AFRL

11. SPONSOR/MONITOR'S REPORT NUMBER(S)
AFRL-VS-HA-TR-2005-1031

12. DISTRIBUTION / AVAILABILITY STATEMENT
Approved for Public Release; Distribution Unlimited.

13. SUPPLEMENTARY NOTES

*** Science Applications International Corporation** ***** Institute for the Dynamics of the Geospheres**

**** NORSAR**

14. ABSTRACT

We analyze data from two sets of decoupled chemical explosions. NORSAR has obtained data from 15 decoupled chemical explosions conducted from 1986-2002 in Älvdalen, Sweden, on regional seismic stations NORES, HFS, and NORSAR. The explosions were conducted in three nonspherical granite chambers at a depth of approximately 100 meters in chambers with volumes of 200, 300 and 1000 m3 and yields ranging from 500 kg to 10,000 kg. The smallest explosions in the largest chamber are fully decoupled, while the other explosions are partially coupled, overdriven by up to a factor of 25. The data show that decoupling remains fairly constant for overdrive up to about a factor of 10, then decreases rapidly at higher yields. Several 1,000 kg explosions were conducted in the two smaller chambers. These events did not appear in seismic bulletins, however, we were able to identify the waveform and estimate the origin time using a waveform correlation procedure. For the more recent explosions, near field data were recorded on pressure gauges in the chamber and adjacent tunnel, and on velocity gauges in boreholes at several locations near the chamber. We modeled these data using three-dimensional finite difference calculations. The calculations show enhanced signals in the direction along the small axis of the chamber and reduced signals near the long end of the tunnel. Although we do not have free field data from all directions, the data for the available locations are consistent with these calculations.

15. SUBJECT TERMS
Seismic propagation

16. SECURITY CLASSIFICATION OF:			17. LIMITATION OF ABSTRACT	18. NUMBER OF PAGES	19a. NAME OF RESPONSIBLE PERSON
a. REPORT	b. ABSTRACT	c. THIS PAGE			Robert J. Raistrick
UNCLAS	UNCLAS	UNCLAS	SAR	59	19b. TELEPHONE NUMBER *(include area code)* 781-377-3726

Standard Form 298 (Rev. 8-98)
Prescribed by ANSI Std. 239.18

ABSTRACT

We analyze data from two sets of decoupled chemical explosions. NORSAR has obtained data from 15 decoupled chemical explosions conducted from 1986-2002 in Älvdalen, Sweden, on regional seismic stations NORES, HFS, and NORSAR. The explosions were conducted in three nonspherical granite chambers at a depth of approximately 100 meters in chambers with volumes of 200, 300 and 1000 m^3 and yields ranging from 500 kg to 10,000 kg. The smallest explosions in the largest chamber are fully decoupled, while the other explosions are partially coupled, overdriven by up to a factor of 25. The data show that decoupling remains fairly constant for overdrive up to about a factor of 10, then decreases rapidly at higher yields. Several 1,000 kg explosions were conducted in the two smaller chambers. These events did not appear in seismic bulletins, however, we were able to identify the waveform and estimate the origin time using a waveform correlation procedure. For the more recent explosions, near field data were recorded on pressure gauges in the chamber and adjacent tunnel, and on velocity gauges in boreholes at several locations near the chamber. We modeled these data using three-dimensional finite difference calculations. The calculations show enhanced signals in the direction along the small axis of the chamber and reduced signals near the long end of the tunnel. Although we do not have free field data from all directions, the data for the available locations are consistent with these calculations.

IDG has digitized a set of surface seismic data recorded from a series of Soviet high-explosive cavity decoupling tests conducted in a mine in Kirghizia in the summer of 1960. These decoupled tests were carried out in a variety of mined cavities in limestone with the objectives of assessing the dependence of cavity decoupling effectiveness on cavity volume, cavity shape, and charge emplacement geometry. New data from these tests at distances of 5 and 10 km from the source augment earlier data from near field records of these explosions, allowing the frequency dependence of the decoupling factor to be measured. The decoupled tests conducted in the center of the cavities show low frequency chemical decoupling factors in the range 20-30, while that conducted 1 m from the wall of the 4.92 m radius cavity is about a factor of two smaller, indicating increased seismic coupling associated with nonlinear response of the cavity wall. Decoupling factors decrease to less than 10 at high frequency.

TABLE OF CONTENTS

LIST OF FIGURES

Figure **Page**

List of Figures (Continued)

Figure **Page**

List of Figures (Continued)

Figure **Page**

List of Figures (Continued)

Figure **Page**

ix

LIST OF TABLES

Table **Page**

PREFACE

The explosions discussed in section 3 of this report were conducted in a cooperative effort between the Norwegian Defense Building and Infrastructure Agency (Forsvarsbygg), Defense Science & Technology Agency (DSTA) of Singapore and the Swedish Defense Research Agency. The lead agency of the large scale tests, DSTA, and the other participants, kindly provided the data. We thank them for their support and for the use of their data.

1 EXECUTIVE SUMMARY

The objective of this project is to improve our capability to predict quantitatively the decoupling effectiveness of underground cavities in a variety of realistic configurations. This is accomplished by expanding the existing decoupling data set with data that have recently become available from Russian and Swedish decoupled chemical explosions, and by performing data analysis and numerical modeling of this data set. This is a joint project of Science Application International Corporation (SAIC), the Russian Institute for the Dynamics of the Geospheres (IDG), and NORSAR.

Although cavity decoupling has been the subject of extensive study over a period of nearly 40 years, there is still considerable quantitative uncertainty in the decoupling factor – the ratio of coupled to decoupled seismic signal that can be achieved under different conditions. This uncertainty comes from three sources – first, there is only a limited amount of decoupled data available; second, there is considerable uncertainty in the low pressure equation of state used in numerical modeling of decoupled explosions; and third, there has been only a limited investigation of the effectiveness of decoupling by nonspherical cavities. In this report, we analyze and model two data sets provided by NORSAR and IDG. Our primary interest is to investigate:

1) the chemical decoupling effectiveness of the rectangular chamber in granite for a range of partially coupled yields; and
2) the amplitude and frequency dependence of chemical decoupling in the limestone cavity experiments.

NORSAR obtained data from 15 decoupled chemical explosions conducted from 1986-2002 in Älvdalen, Sweden. All but two of the explosions were recorded by the NORES and NORSAR arrays. The last explosion occurred shortly after NORES was damaged by lightning. The last six were also recorded on the HFS array in Sweden. NORSAR participated in the explosions during the summer of 2001 and 2002. They deployed a number of temporary instruments including one surface instrument for each event on site near the explosion. The last five explosions were conducted in a cavity approximately 4 meters high by 8 m wide by 30 m long (1000 m^3). The first ten explosions were in two smaller chambers approximately 3 meters high by 4 meters wide with lengths of 17 meters (200 m^3) and 25 meters (300 m^3). Explosive yields ranged from 500 kg to 10,000 kg, with charges consisting of TNT, ANFO and ammunition shells. The smallest two explosions in the largest chamber appear to be fully decoupled, while the other explosions are partially coupled. A potentially important observation for monitoring is that even the fully decoupled 2500 kg explosion was detected at NORSAR, at a distance of about 150 km. The fully decoupled 500 kg explosion was detected using waveform correlation, however, the signal/noise ratio was too low for any additional analysis.

The results of the decoupling analysis are summarized in Figure 1 which shows observed chemical decoupling factors for the Swedish chamber explosions together with predicted chemical decoupling factors for a spherical cavity of the same volume. The decoupling factor contains an unknown scale factor, since we do not have data from a tamped explosion for comparison. The horizontal axis corresponds approximately to the overdrive factor above full decoupling. Both the data and the simulation show that the explosion remains nearly fully decoupled until the yield is increased

by about an order of magnitude above the yield required for full decoupling. However, the decrease occurs at a lower yield for the observations than for the calculations, which is expected since the smallest dimension of the chamber is considerably closer to the explosion, and therefore is impacted by a stronger shock, than the wall of the equivalent volume spherical cavity.

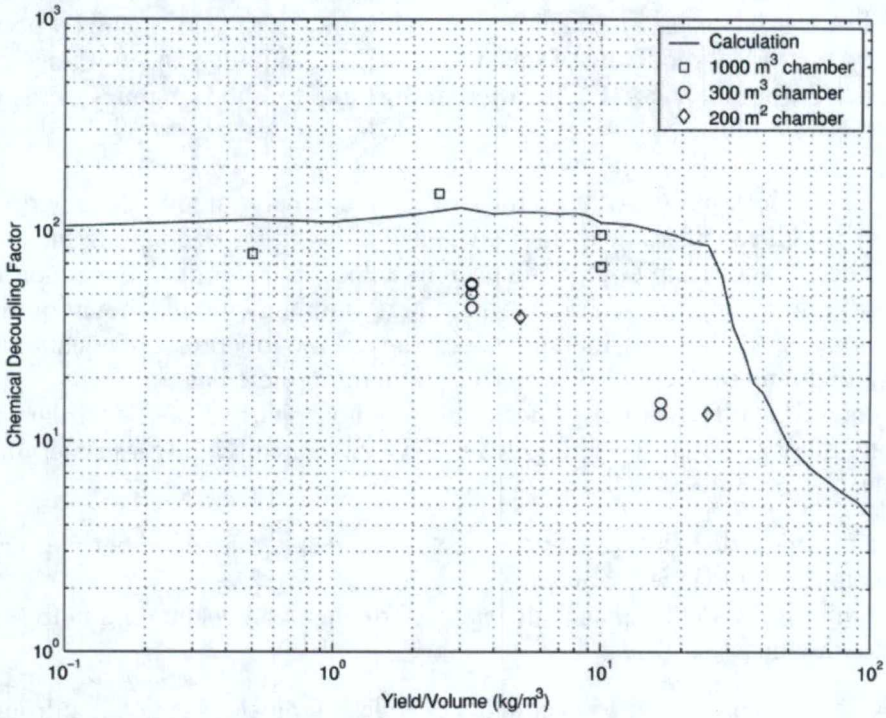

Figure 1. Observed and predicted chemical decoupling factor for Swedish chamber explosions. The Swedish explosions were in rectangular chambers in granite with volumes of 200 m^3, 300 m^3 and 1000 m^3. The calculations were for a chemical explosion in a 6.3 meter spherical cavity in granite (1000 m^3).

Near field data from three events were recorded on pressure gauges in the chamber and adjacent tunnel, and on velocity gauges in boreholes at several locations near the chamber. We performed data analysis of waveforms and spectra at the arrays, and both one-dimensional and three-dimensional numerical modeling of the near field data. The 3D nonlinear calculations of the chamber explosions show strong nonlinearity at the points closest to the explosion. Calculations show stronger near field waveforms in this direction, with reduced amplitudes off the ends of the chamber where the measurements were made that are consistent with the observed data.

In addition to the Älvdalen data, NORSAR also collected data from decoupled explosions in mine shafts at Løkken Gruver. This data set was collected near the end of the project so only a very limited amount of data analysis has been performed with it. However, because of the large number of continuing decoupled explosions at this site, it is a potentially excellent source of additional decoupled explosion data.

IDG digitized a set of surface seismic data recorded from a series of Soviet high-explosive cavity decoupling tests conducted in a mine in Kirghizia in the summer of 1960. These decoupled tests were carried out in a variety of mined cavities in limestone with the objectives of assessing the

dependence of cavity decoupling effectiveness on cavity volume, cavity shape, and charge emplacement geometry. In a previous study, Murphy et al (1997) conducted extensive analyses of free-field data recorded from these tests in the mine at distances on the order of 10-200 m. However, only limited waveform data were available from this regime, which made it difficult to determine the frequency dependence of the decoupling factors with a high degree of confidence. In the present study, seismic data recorded from a number of these tests on the surface at distances of 5 and 10 km from the source region have been recovered and digitized.

We analyzed the digitized 3-component seismic data that was recorded at surface stations located 5 and 10 km away, and compared these results with those obtained earlier from close-in data (Figure 2). High quality recordings are available from the 1 ton tamped and decoupled tests at the 5 km station, and the 6-ton tamped and decoupled tests at the 5 and 10 km stations. Results of detailed analyses of these data are consistent with those obtained from the previous analysis of the corresponding free-field data. In particular, all the decoupled tests conducted in the center of the cavities show low frequency chemical decoupling factors in the range 20-30, while that conducted 1 m from the wall of the 4.92 m radius cavity is about a factor of two smaller, indicating increased seismic coupling associated with nonlinear response of the cavity wall. The seismic signals observed from the 1 ton explosions conducted at the centers of the 2.88 m and 4.92 m radius cavities were found to be nearly identical, confirming that both of these tests were fully decoupled.

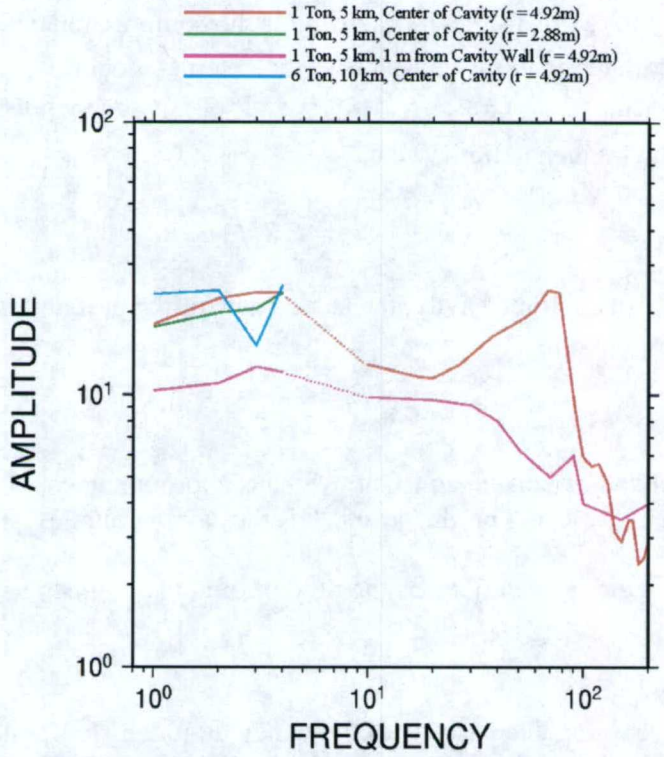

Figure 2. Frequency dependent chemical decoupling factors for the 1 and 6 ton tests at the 5 and 10 km stations. Also shown are the corresponding results at higher frequency (10 – 200 Hz) obtained previously by Murphy et al (1997) from the corresponding free-field data.

2 INTRODUCTION – DECOUPLING THEORY AND CRITERIA FOR FULL DECOUPLING

The source function for a fully decoupled explosion can be described as a pressure pulse applied to the wall of a cavity in an elastic medium. The actual physics is more complicated than this – there are reverberations in the cavity that cause high frequency spectral peaks, and the shock wave that hits the wall is stronger than an instantaneously applied pressure pulse corresponding to a uniformly pressurized cavity. However the simple model is useful for illustration and has many of the characteristics of a decoupled explosion. This simple description is also applicable to non-spherical cavities, however non-spherical cavities will become partially coupled at smaller yields because the smallest cavity dimension is closer to the source and will be impacted by a stronger shock wave than the spherical cavity.

The reduced velocity potential (RVP) for a pressure pulse $P(t)$ with derivative $\dot{P}(t)$ and corresponding Fourier transforms $P(\omega)$ and $\dot{P}(\omega)$ applied to the wall of a spherical cavity is (Stevens et al, 1991):

$$\dot{\psi}(\omega) = \dot{P}(\omega)\frac{R^3\omega_0^2}{4\mu}\frac{e^{i\omega/\omega_0}}{\omega_0^2 + i\omega\omega_0 - \left[(\lambda+2\mu)/4\mu\right]\omega^2} \tag{1}$$

where $\omega_0 = \alpha/R$, where R is the cavity radius, α is the compressional velocity of the external medium and λ and μ are the Lame constants of the external medium. For a step in pressure of magnitude P_0 applied at time $t = 0$, $\dot{P}(\omega) = P_0$, and for this or any pressure pulse with static value P_0, in the low frequency limit, we have

$$\psi_\infty = P_0 R^3/4\mu \tag{2}$$

For an explosion in an air-filled cavity, the static value of the pressure is related to the yield W by

$$P_0 = \frac{(\gamma-1)W}{V} \tag{3}$$

where γ is the adiabatic expansion constant, which is approximately 1.2 for strong shocks in air and 1.3 for chemical explosion products, and V is the cavity volume.

The "decoupling factor" D is defined as the ratio of the fully coupled to decoupled source:

$$D = \psi_{tamped}/\psi_{decoupled} \tag{4}$$

The theoretical decoupling decreases with frequency. Figure 3 shows the coupled and decoupled source function and the frequency dependent decoupling factor obtained by taking the ratio of coupled to decoupled source for a 10 ton explosion. The decoupling factor decreases by an order of magnitude at high frequencies beginning at about 10 Hz. This decline is initially due to the shape of the tamped spectrum, as the decoupled spectrum is flat to approximately 100 Hz.

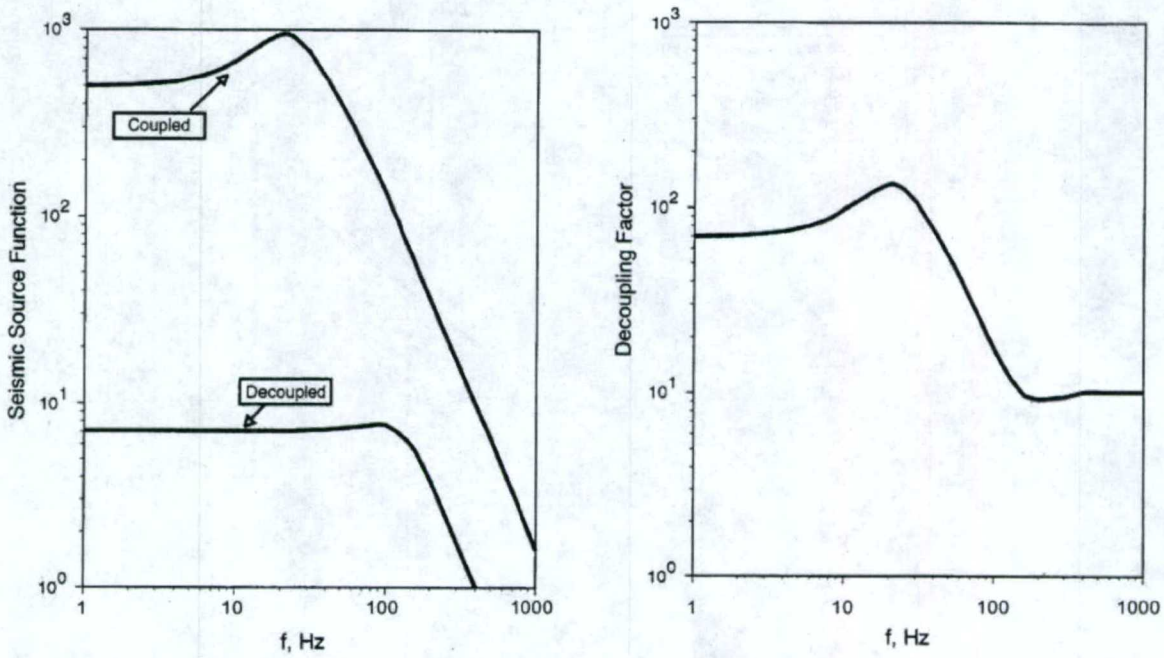

Figure 3. Source functions for fully coupled and fully decoupled 10 ton chemical explosions for a step pressure source in the cavity (left) and frequency dependent decoupling factor (right).

The approximate criterion for full decoupling is usually expressed in terms of a requirement that the late-time, equilibrium pressure in the cavity be less than or equal to some constant, k, times the overburden pressure (Herbst et al, 1961):

$$\frac{(\gamma-1)W}{V} \leq k\rho gh \tag{5}$$

where k is between 0.5 (Latter) and 1.0 (Patterson), and ρgh is the overburden pressure at depth h. The Swedish chamber explosions discussed in Section 3 of this report are at 100 meters depth in granite. Figure 4 shows the Latter criterion for full decoupling together with the actual parameters calculated from the known depth and volume for each of these explosions. All but one of the explosions exceeds the Latter threshold. The 2500 kg explosion in the 1000 m^3 chamber is also close to fully decoupled.

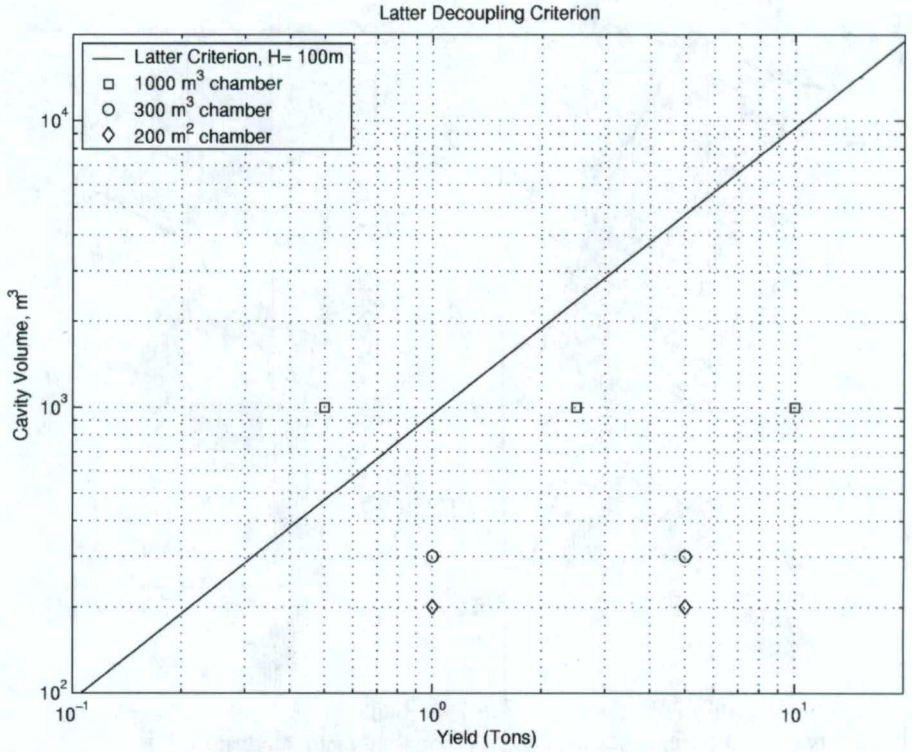

Figure 4. Latter decoupling criterion calculated for the conditions of the Swedish chamber explosions. The actual values for the Swedish chamber explosions are marked.

3 DECOUPLED EXPLOSIONS AT ÄLVDALEN, SWEDEN

At a site within Älvdalen Skjutfält in central Sweden, 15 decoupled chemical explosions have been carried out within underground cavities at a depth of approximately 100 meters. The site is approximately equidistant from the seismic arrays HFS (Hagfors, Sweden), NRS (NORES, Norway), and the wide aperture NORSAR array (Figure 5). Data from surface explosions at Mossibränden, which is located a few km from Älvdalen, were analyzed in an earlier report (Stevens et al, 2002) and compared with data from the decoupled explosions.

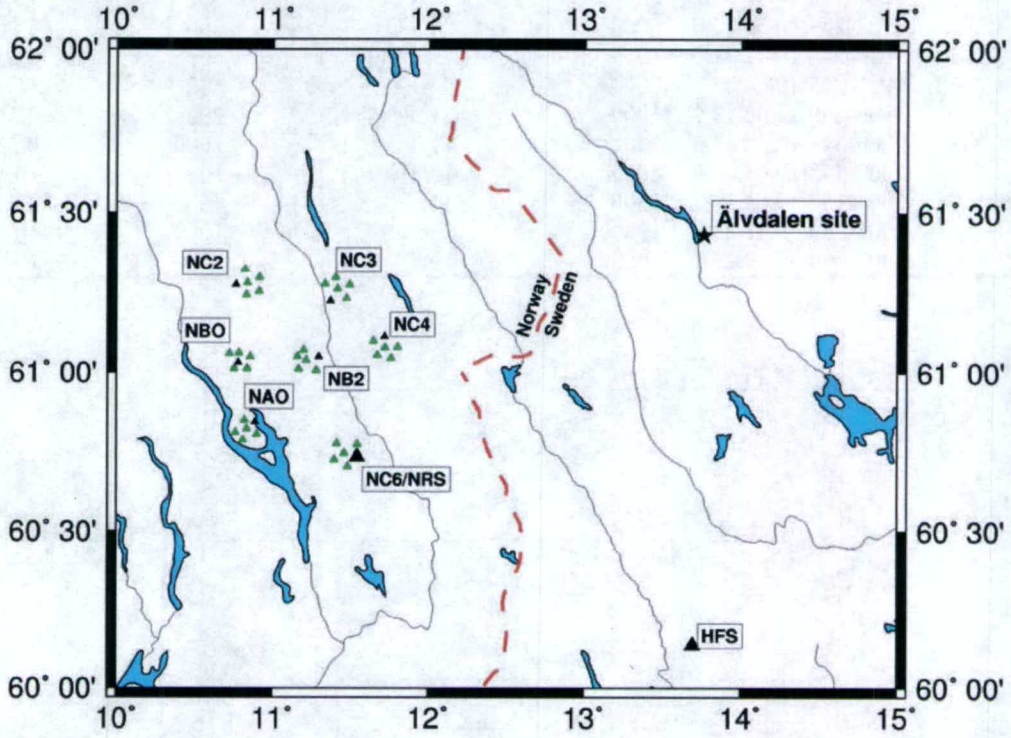

Figure 5. The location of the explosion site relative to the HFS and NORES (NRS) arrays and the seven NORSAR sub-arrays. The dashed line is the Norway/Sweden national boundary.

3.1 Decoupled Chamber Explosions

The cavity explosions, which comprise two separate series of experiments (1987-96 and 2000-2002) are listed in Table 1. The set of events from the underground cavities includes 3 different quantities of explosives in nearly co-located chambers of 3 different sizes. All chambers are open to the same tunnel system. The 2000-2002 series of explosions were conducted in a cavity approximately 4 meters high by 8 m wide by 30 m long (1000 m^3). The 1987-1996 explosions were in two smaller chambers approximately 3 meters high by 4 meters wide with lengths of 17 meters (200 m^3) and 25 meters (300 m^3) as shown in Figure 6. A photograph of the ammunition shells detonated in the 1996 explosion is shown in Figure 7.

Table 1. Cavity decoupled chemical explosions at the Älvdalen site. Origin times of the last four 2000-2002 events were determined from a station at the explosion site. Origin times of earlier events were determined by waveform correlation with data from the later events.

Origin ID	Explosion origin time	Explosion charge (kg)	Explosive	Chamber Volume (m^3)	Charge/Volume (kg/m^3)
1986C168	1986-168:10.06.15.9	1000	TNT	300	3.3
1986C177	1986-177:09.14.06.6	1000	TNT	200	5.0
1986C246	1986-246:11.50.45.1	1000	Shells (TNT)	200	5.0
1986C260	1986-260:11.34.17.4	1000	Shells (TNT)	300	3.3
1987C141	1987-141:10.16.08.3	1000	ANFO	300	3.3
1987C146	1987-146:10.47.38.2	5000	ANFO	300	16.7
1987C259	1987-259:10.36.13.0	5000	ANFO	200	25.0
1989C242	1989-242:10.12.21.0	1000	Shells (TNT)	300	3.3
1989C263	1989-263:10.06.03.5	5000	ANFO	300	16.7
1996C269	1996-269:11.00.13.9	1000	Shells (TNT)	300	3.3
2000C343	2000-343:10.43.04.5	500	TNT	1000	0.5
2000C348	2000-348:10.03.02.0	10000	TNT	1000	10
2001C150	2001-150:10.03.56.2	2500	TNT	1000	2.5
2001C186	2001-186:10.41.23.5	10000	Shells (TNT)	1000	10
2002C164	2002-164:08.59.25.1	10000	TNT/powder	1000	10

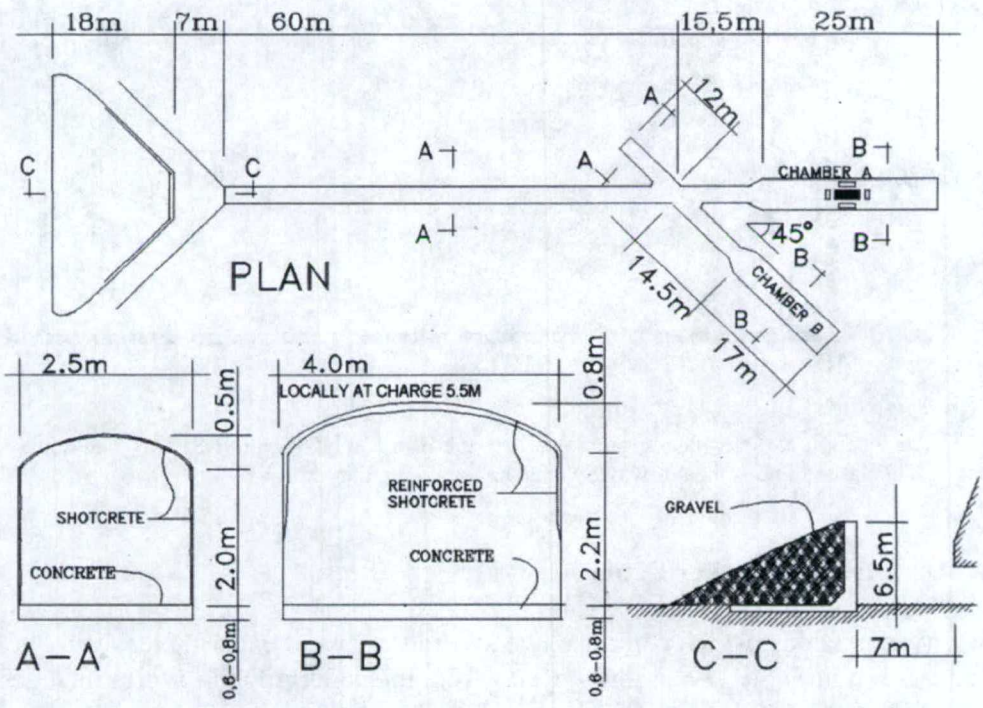

Figure 6. Geometry of the smaller chambers A and B in the Älvdalen tunnel complex which were used for the Klotz explosions between June 1986 and September 1989. Chamber A was widened slightly before the explosion of September 1996 (from Hansson and Forsén, 1997).

Figure 7. Photograph of explosive set up for the September, 1996 detonation (from Hansson and Forsén, 1997).

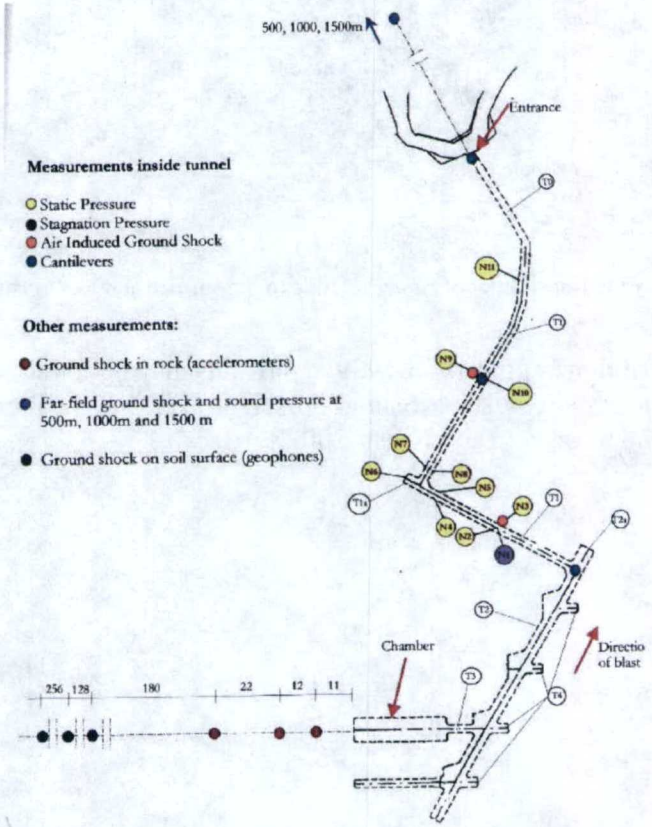

Figure 8. Location of the 1000 m^3 chamber in relation to the entrance and the pressure sensors in the access tunnels.

Figure 8 shows the location of the large chamber, the adjacent tunnel complex, and the location of pressure sensors and accelerometers that recorded data from the explosions. The entrance to all of the chambers is open, so the blast wave from the chamber explosions propagate out of the chamber and down the tunnel. Since the open tunnel depressurizes the chamber, analysis based on a closed chamber is only valid up to a time corresponding to the characteristic decay time associated with venting of cavity pressure down the tunnel. Figure 9 shows the location of the underground chamber relative to the surface and local instrumentation.

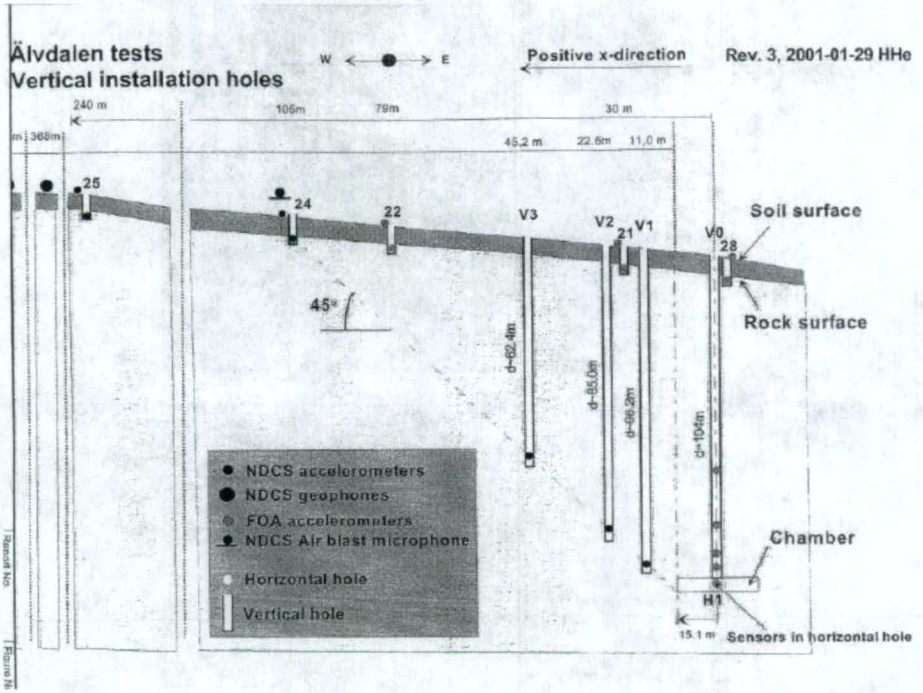

Figure 9. Location of chamber relative to the surface and local instrumentation.

More detailed descriptions of the 1986-1989 explosions may be found in Vretblad (1991). The 1996 explosion is described by Hansson and Forsén (1997), and the recent explosions by Grønstein (2000) and Grønstein and Krest (2002).

3.2 Regional Data for Decoupled Chamber Explosions

The largest seven events were all detected at the regional seismic arrays that were in operation at the time of the event. The data available for each event is shown in Table 2. The NORSAR (NOA) array was upgraded from 20 to 40 Hz sampling in 1995. NORES (NRS) was destroyed by lightning on June 11, 2002, two days prior to the last explosion.

Table 2. Data availability for the 15 decoupled explosions.

Origin ID	Explosion charge (kg)	Chamber Volume (m^3)	NOA (20 Hz)	NOA (40 Hz)	NORES (NRS)	HFS (40 Hz)	HFS (80 Hz)
1986C168	1000	300	X		X		
1986C177	1000	200	X		X		
1986C246	1000	200	X				
1986C260	1000	300	X		X		
1987C141	1000	300	X		X		
1987C146	5000	300	X		X		
1987C259	5000	200	X		X		
1989C242	1000	300	X		X		
1989C263	5000	300	X		X		
1996C269	1000	300		X	X	X	
2000C343	500	1000		X	X	X	
2000C348	10000	1000		X	X	X	
2001C150	2500	1000		X	X	X	
2001C186	10000	1000		X	X	X	
2002C164	10000	1000		X		X	X

In addition to the regional arrays, the last four explosions were also recorded by temporary high frequency field instruments placed by NORSAR. Near field measurements, which are described in the next section of this report, were taken for three of the events in 2000 and 2001.

The 500 kg and seven 1000 kg events did not appear in any seismic bulletin and a visual search of the records for the corresponding day (the time was not available) identified only one probable signal. We therefore developed a waveform correlation technique using the event with the largest signal (1987C259) as a master event. The data from this event were cross-correlated with the data for the known day of each event. Arrivals from all six of the 1000 kg events and the 500 kg event were identified using this technique. Figure 10 shows an example for event 1986C177.

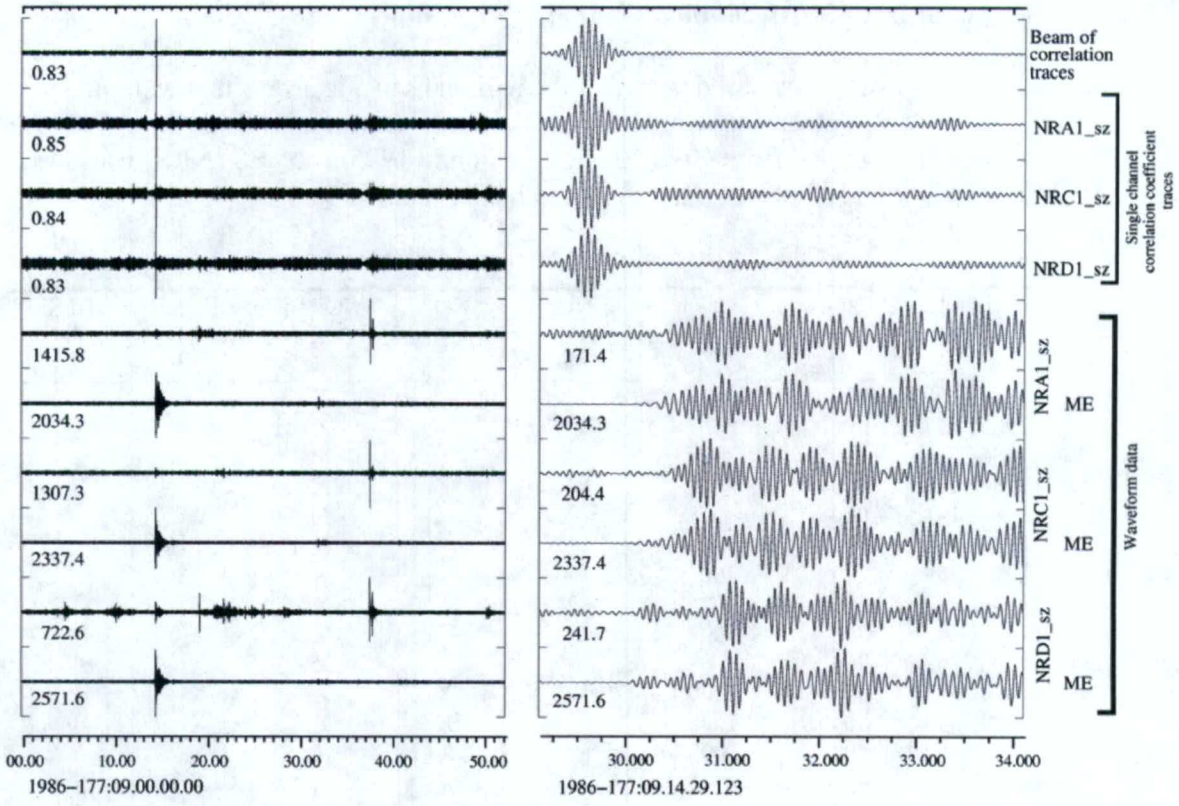

Figure 10. Detection of Älvdalen event 1986C177 using NORES data and waveform correlation with the 1987C259 event signal as a master event (ME). A template of length 60.0 seconds was taken from the 1987 event beginning with the P-phase arrival. Waveforms are bandpass filtered between 14 and 18 Hz. Note the high correlation coefficient in spite of the high frequencies used and in spite of the fact that these two events took place in different chambers. The panels show data from the master event aligned with the 1986 data according to the maximum correlation coefficient. The amplitude of the master event signal is over 10 times that for the 1986 event.

Figure 11 shows unfiltered and filtered waveforms for 13 of the underground explosions in Älvdalen recorded at NORES (the other two events were not recorded at NORES). The signals resulting from three events from 1987 and 1989, which were 5000kg explosions in 200 m^3 and 300 m^3 chambers, have much larger amplitudes than the 10,000 kg events which were in the larger 1000 m^3 chamber in 2000 and 2001. The signal from the 2500kg explosion in the 1000m^3 chamber is indistinguishable from the noise without filtering of the data.

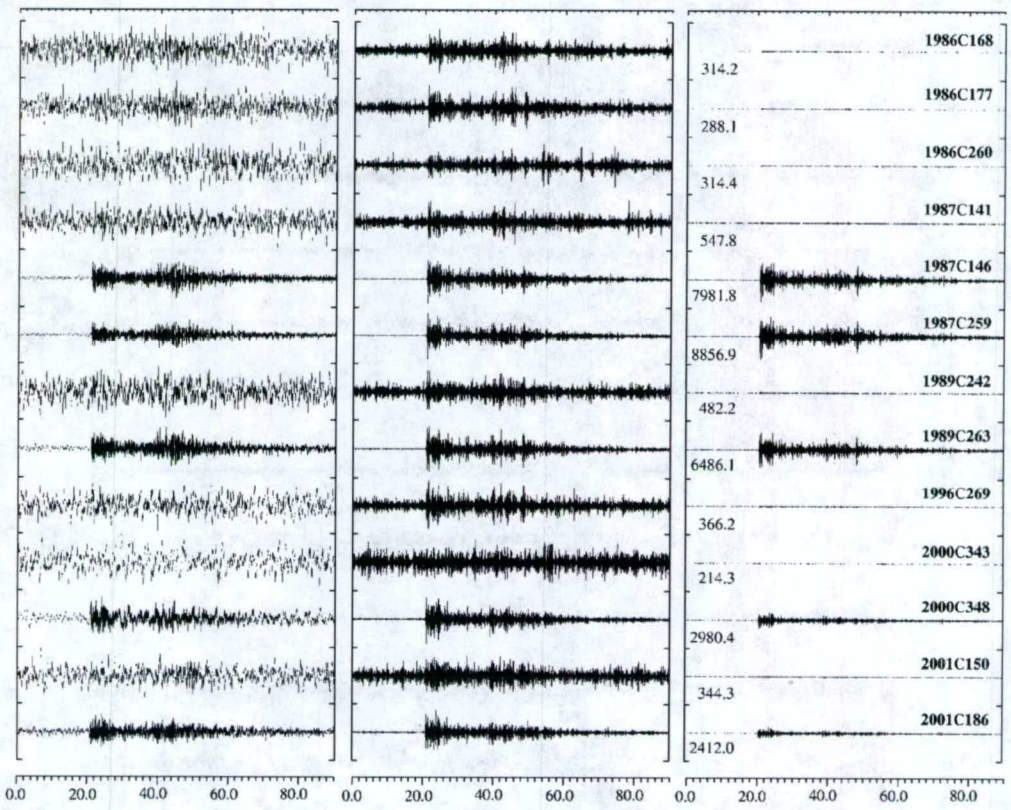

Figure 11. Waveforms from the NORES central element NRA0 (vertical component) for all of the Älvdalen explosions listed in Table 1 (except for events 1986C246 and 2002C164 for which NORES data does not exist). Waveforms are unfiltered in the left hand panel and filtered between 8.0 and 16.0 Hz in the center panel. The filtered waveforms are displayed in the right hand panel to a common vertical scale. Only the events with charge loading density greater than 10 kg/m^3 are visible without filtering, the events with charge density between 2.5 and 5.0 kg/m^3 are detectable using standard array processing when bandpass filtered at high frequencies, and the signal from the 2000C343 event (charge density = 0.5 kg/m^3) is essentially indistinguishable from the noise even with filtering.

In order to quantify the differences between these events, we examine the spectra in three time windows. For each component, time windows were defined corresponding to the P arrival, S arrival, and pre-event noise (Figure 12). A 5 second window of waveform data was extracted immediately after the P onset, and a 10 second window immediately after the S onset. A 10 second window ending 2 seconds before the P onset was defined in order to quantify the level of noise which is expected in the signal.

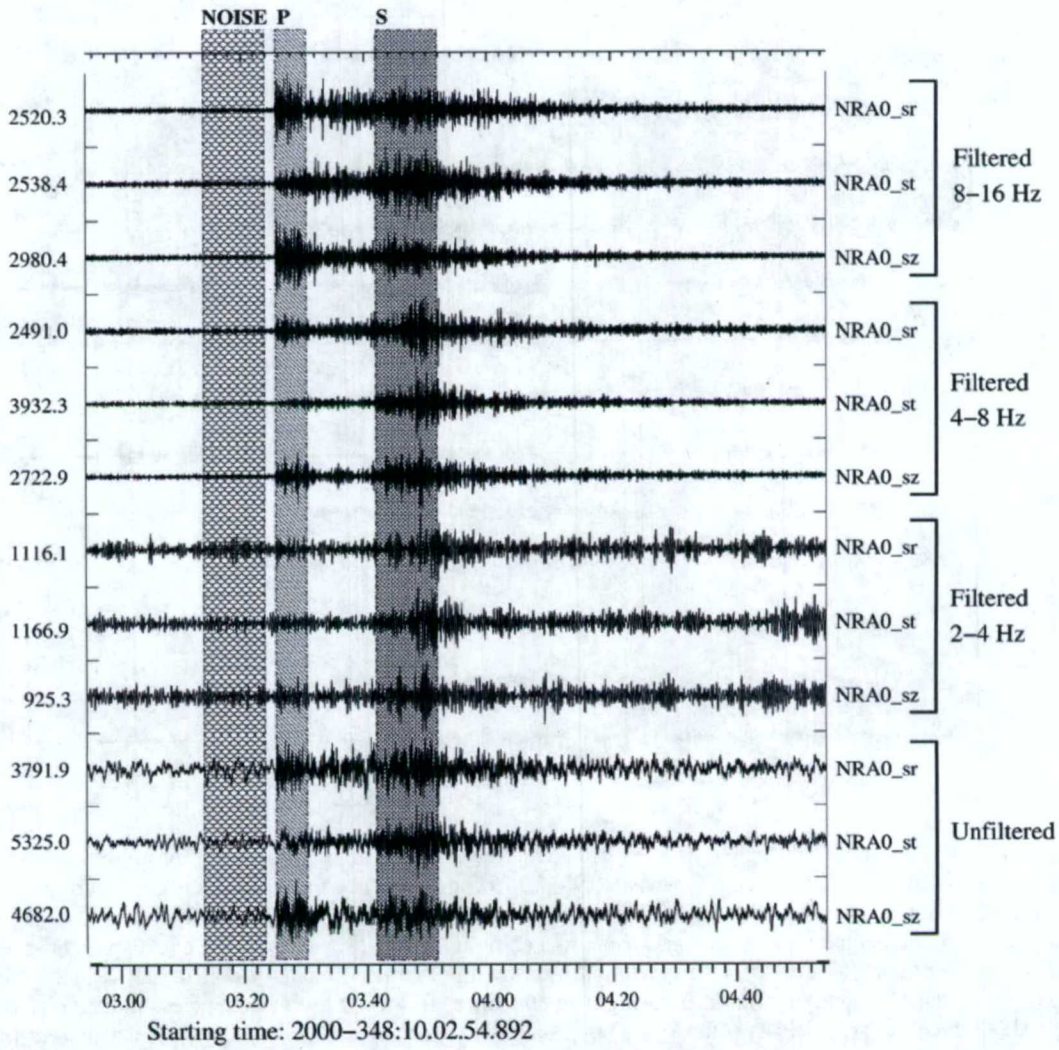

Figure 12. Waveform data for event 2000C348 as recorded by the NORES central instrument, NRA0. The horizontal components are rotated towards the source with a backazimuth of 56 degrees. The lowermost 3 traces are unfiltered data and the remaining traces are filtered with a Butterworth band-pass filter in the frequency bands 2.0 - 4.0 Hz, 4.0 - 8.0 Hz and 8.0 - 16.0 Hz as indicated. Each group of three traces contains the vertical component (z) and the rotated radial (r) and transverse (t) traces. The time windows used to calculate spectra are marked.

Amplitude spectral density was calculated for each time window, with the instrument removed to correct to velocity. The amplitude spectral density was calculated by taking the square root of the power spectral density. Amplitude spectral density, averaged over the vertical components of the NORES array are shown in Figure 13 for the twelve explosions listed in Table 1 that had NORES data, for frequencies up to the Nyquist frequency of 20 Hz. The results shown in Figure 13 clearly show the effect of substantially greater decoupling for the larger chamber relative to the smaller chamber.

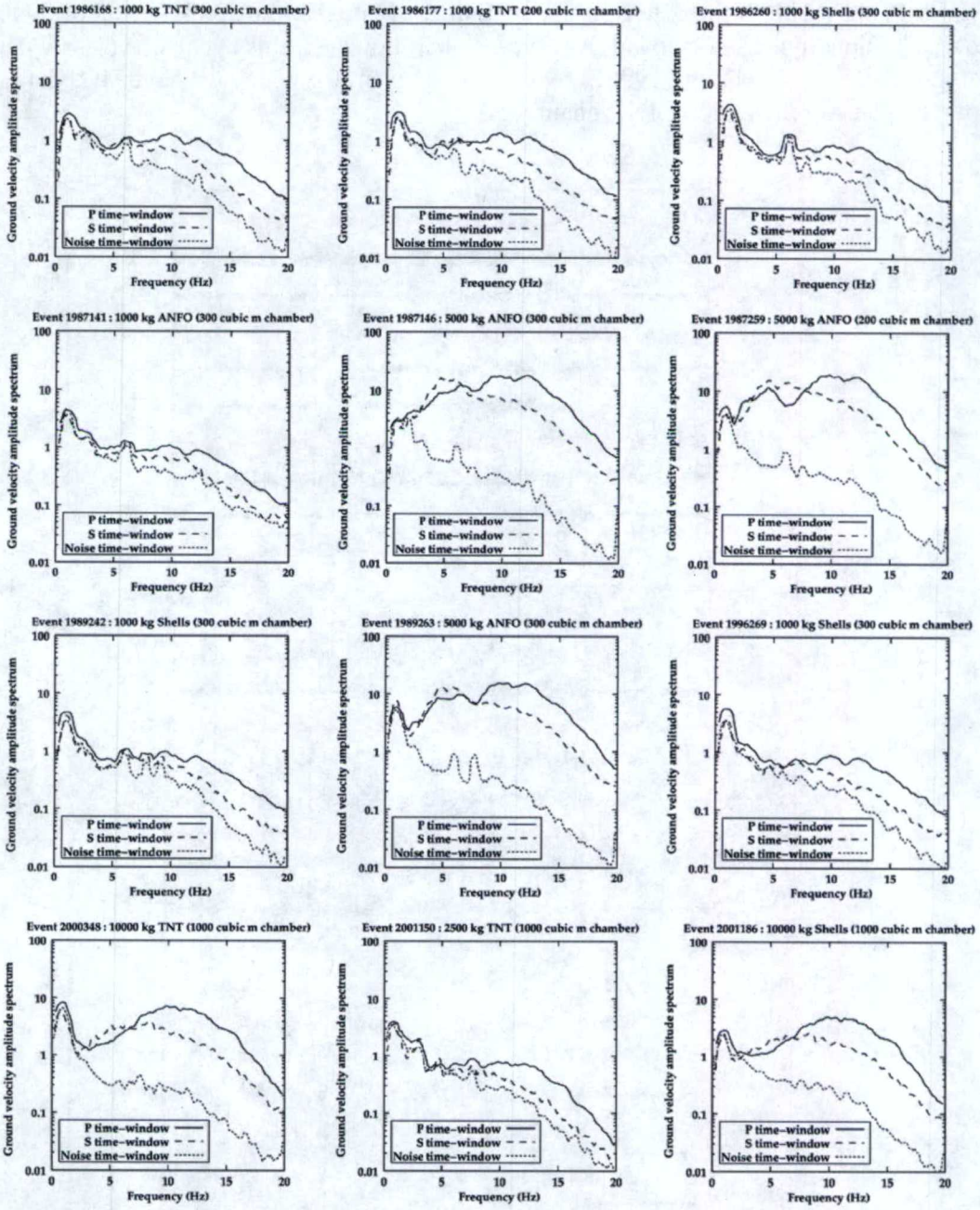

Figure 13. Average amplitude spectral density from NORES vertical component data for the 12 decoupled explosions as indicated; all instrument corrected to velocity. The solid line corresponds to the P window, the dashed line to the S window and the dotted black line to the noise window.

Figure 14 compares data from the NORES center element in several frequency bands from the 1996 explosion with the two tests conducted in 1989. The 1996 and 1000 kg 1989 explosions have comparable, low amplitudes, and are clearly visible only in the 14 to 18 Hz frequency band. The partially coupled 5000 kg explosion generated much stronger signals and is easily visible in the raw data.

Figure 15 shows all of the data from the HFS array. Note that the 500 kg event of 2000C343 is not visible in any frequency band. As noted earlier, however, this event was clearly detected using waveform correlation. 1996C269 is the only event for which we have HFS data which did not take place in the largest of the chambers.

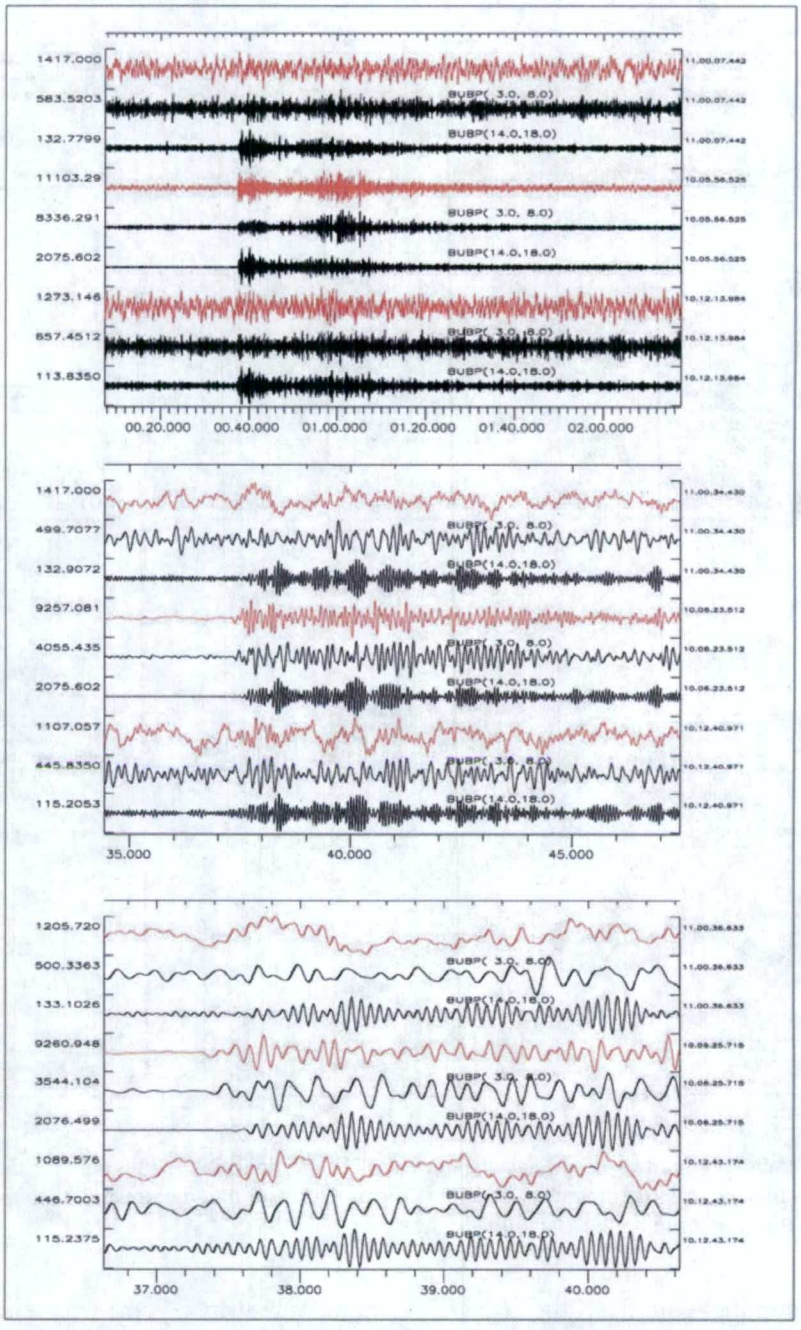

Figure 14. Waveform data for the events 1989C242, 1989C263, and 1996C269 recorded on the NORES center element (channel NRA0_sz). The two lower panels are successive close-ups of the above panel. Each of the three panels contains three triplets of traces; the uppermost corresponding to 1996C269, the middle to 1989C263, and the lowermost to 1989C242. The red traces are unfiltered and the black traces are bandpass filtered as indicated.

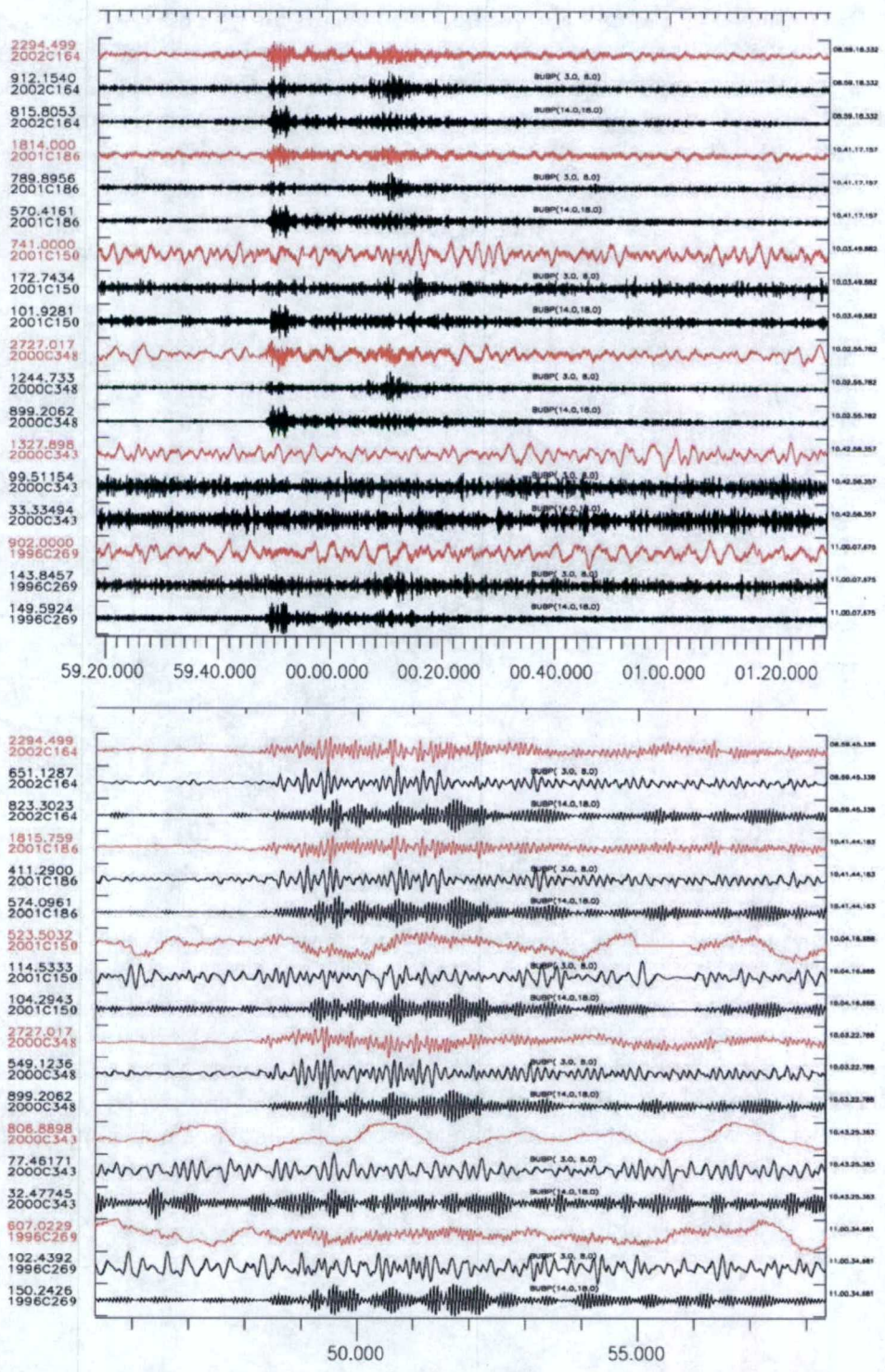

Figure 15. Waveform data from the HFS center element (channel HFSA1_sz) for all of the Älvdalen events for which there exists data from this array. Events are indicated to the side of the traces.

Figure 16 shows NORES amplitude spectra for all events for which NORES data exists and is measurable in the 10-20 Hz frequency band. Each line in the figure is the arithmetic mean of a spectrum calculated using the Thomson multitaper method (Thomson, 1982) from each of the available NORES short period channels in an 8.0 second time window beginning at the first P arrival. Spectra are corrected to velocity.

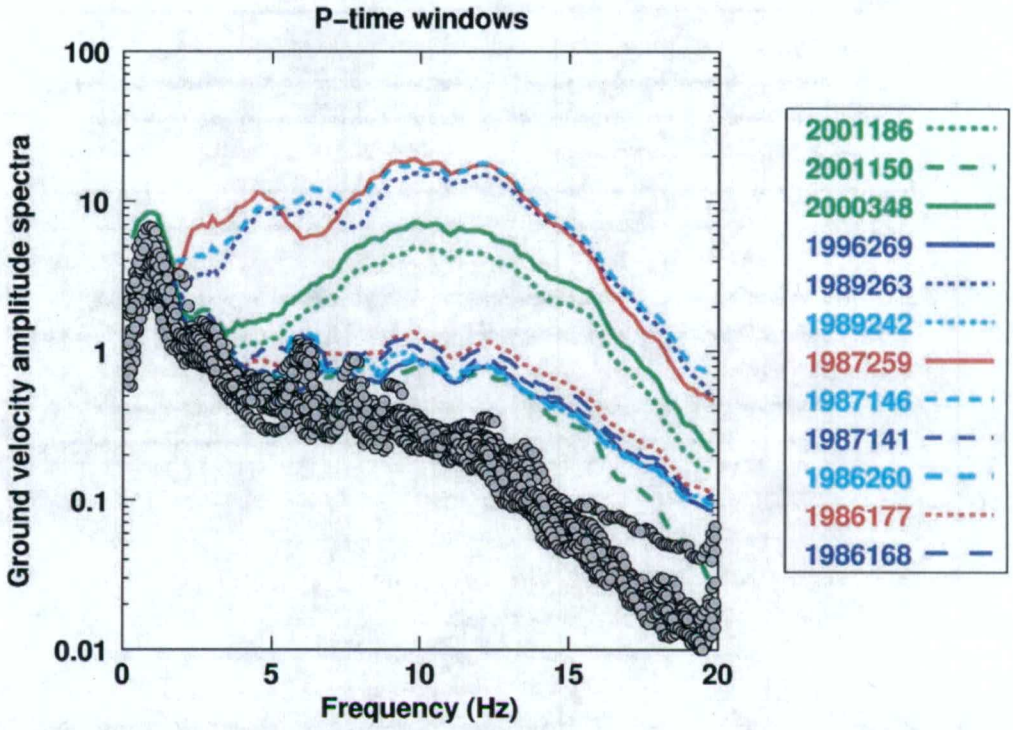

Figure 16. Amplitude spectra from the Älvdalen explosions for which NORES data exists. Green lines are for events which took place in the 1000m^3 chamber, blue lines are for events which took place in Chamber A (300m^3), and red lines are for events which took place in Chamber B (200m^3). Circles show noise measurements for all events.

Figure 17 shows the amplitude scaled by yield and plotted against the charge density in the chamber. The figure shows a clear increase in coupling with charge density for explosions in the same chamber. However, for the same change density, the larger chamber appears to decouple substantially better than the smaller chambers.

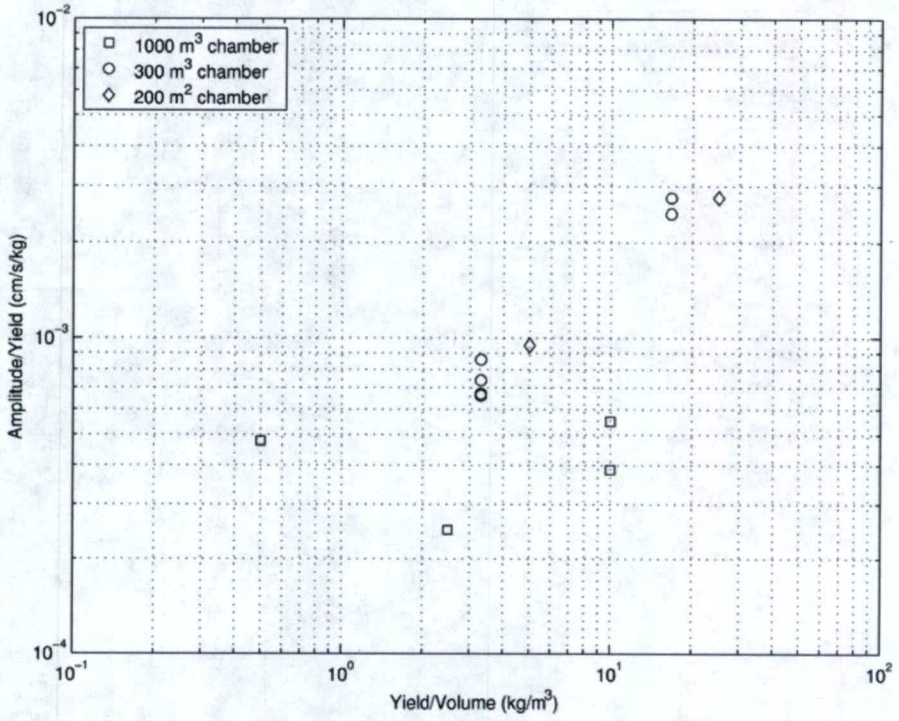

Figure 17. Yield scaled amplitude plotted vs. charge density (yield divided by chamber volume).

3.3 Near Field Recordings (Accelerograms and Pressure Recordings) From the Decoupled Älvdalen Explosions

Near-field accelerometer recordings have been made available by the Norwegian Defence Building and Infrastructure Agency (Forsvarsbygg) for the decoupled explosions in 2000 and 2001 (2000C348, 2001C150 and 2001C186 in Table 1), with additional pressure measurements from within the detonation chamber for the two decoupled explosions in 2001. All of these tests were conducted in the 4x8x30 meter (1000 m^3) chamber.

3.3.1 Accelerograms

The acceleration data consists of three-component recordings in vertical boreholes and two two-component (vertical + parallel to long axis of chamber) at soil and rock sites. The boreholes are located at distances of 11, 22.6 and 45.2 m west of the chamber wall, while the surface accelerometers have an assumed location 96.5 m west (assumed along the same line) of the chamber wall. The accelerometer locations relative to the detonation chamber are shown in Figure 18.

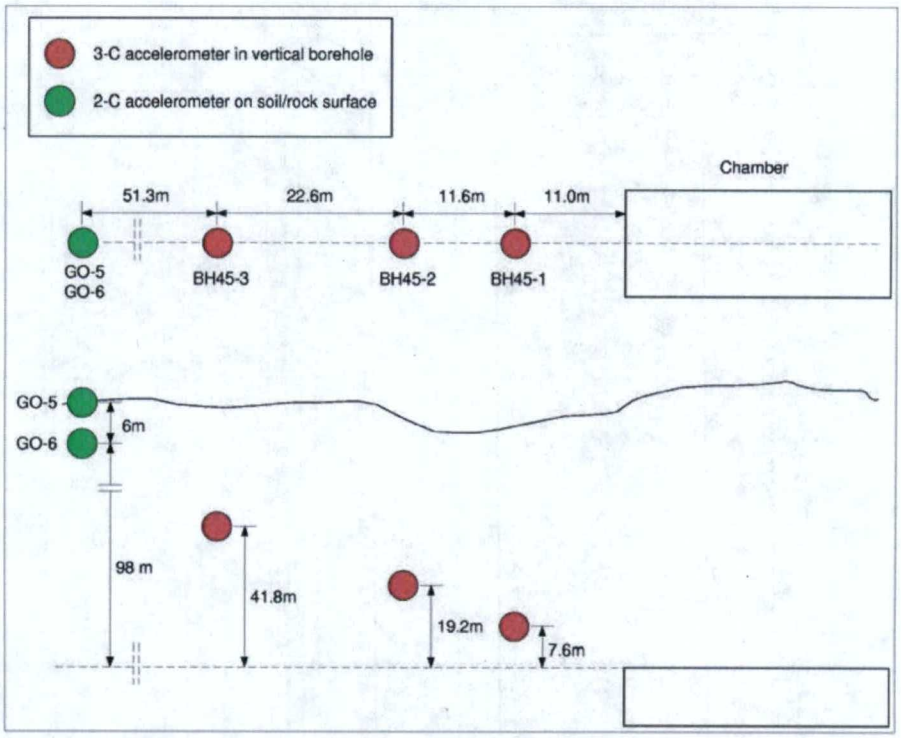

Figure 18. Accelerometer configuration relative to detonation chamber. Note that BH45-1,2,3 correspond to locations V1, V2 and V3.

Raw data for each of the three explosions is shown in Figure 19 – Figure 21, and filtered comparisons of the three explosions at the same station are shown in Figure 22 – Figure 25. Note that the peak amplitude is approximately proportional to yield at common stations.

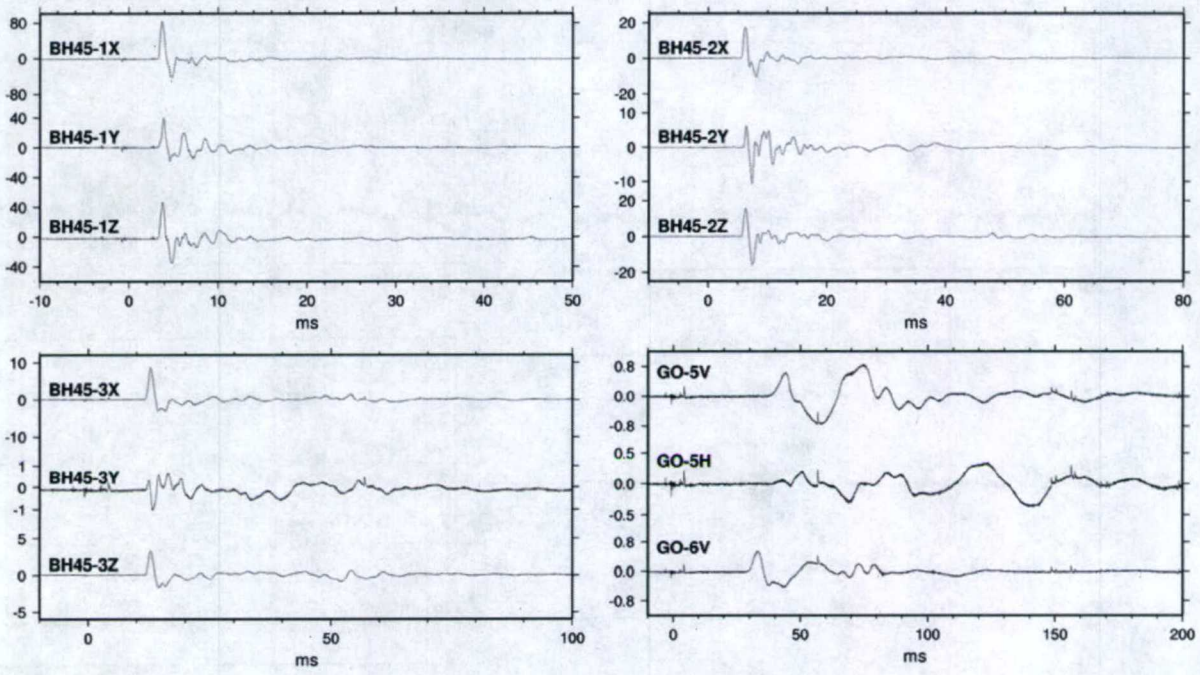

Figure 19. Near-field accelerometer recordings of the 10,000 kg TNT explosion on December 13, 2000 (2000C348). Vertical scale is in g.

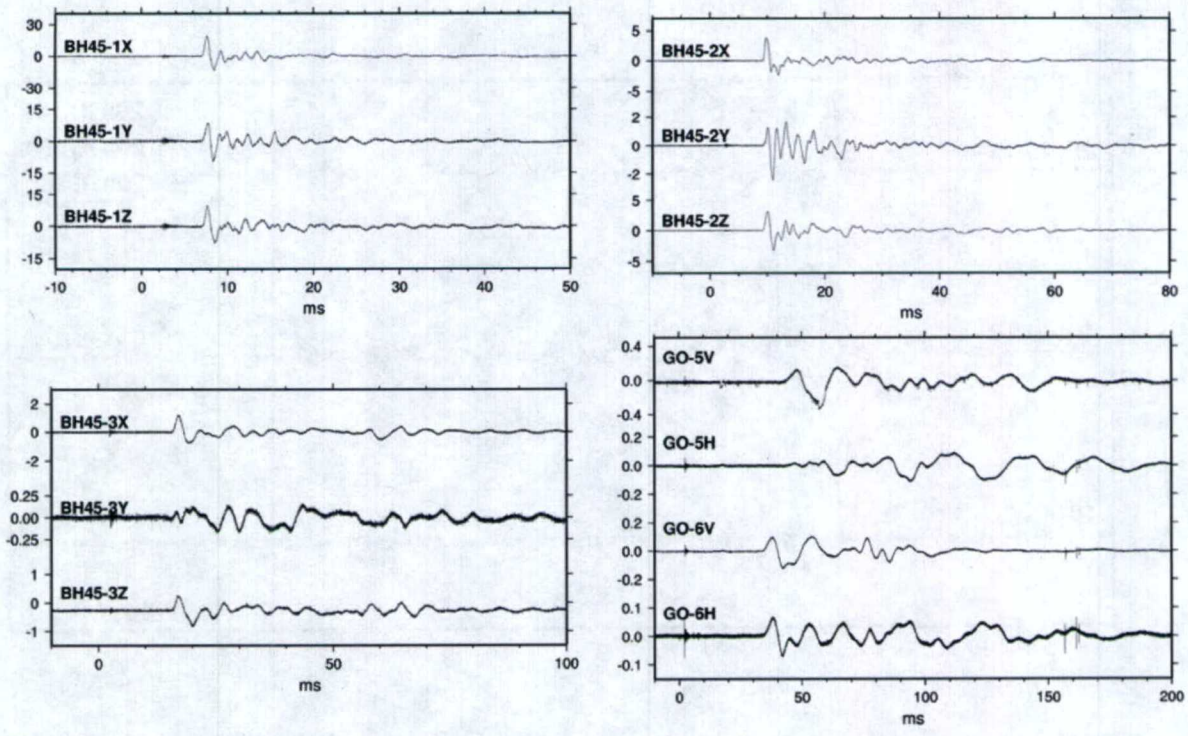

Figure 20. Near –field accelerometer recordings of the 2,500 kg TNT explosion on May 30, 2001 (2001C150). Vertical scale is in g.

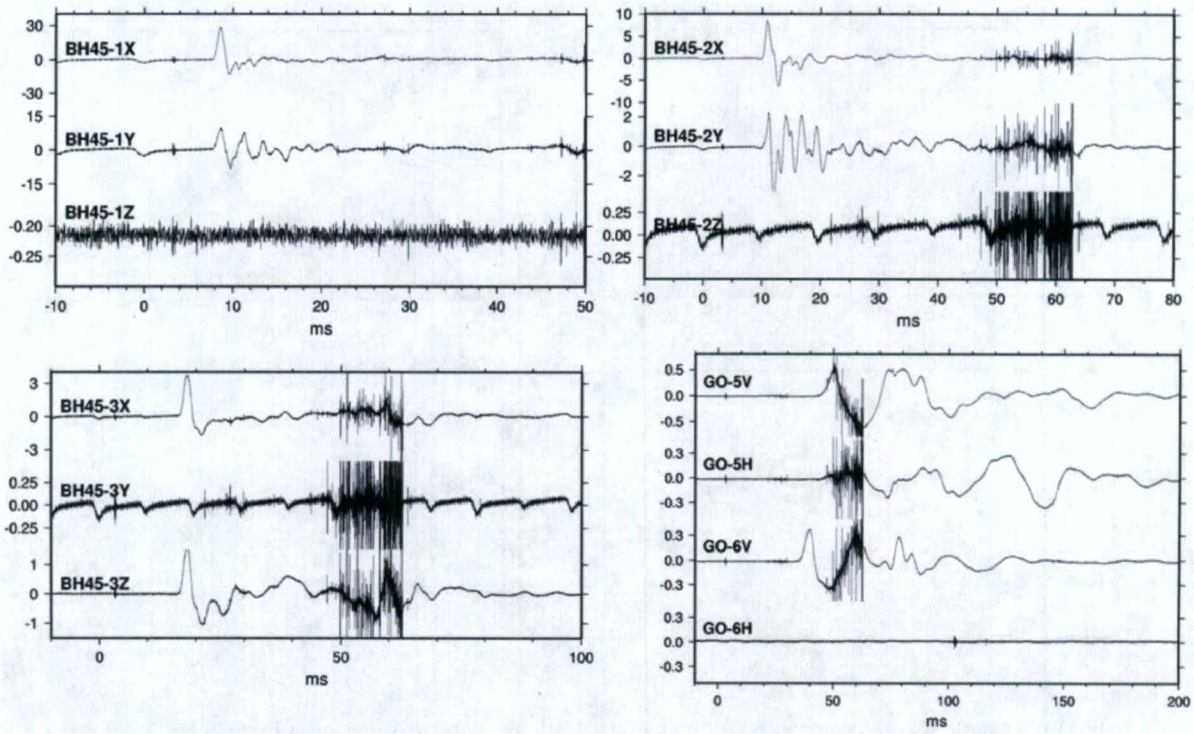

Figure 21. Near-field accelerometer recordings of the 10,000 kg ammunition shell explosion on July 5, 2001 (2001C186). Vertical scale is in g. Note the significantly lower accelerations compared to the 10,000 kg TNT explosion on December 13, 2000 in Figure 19.

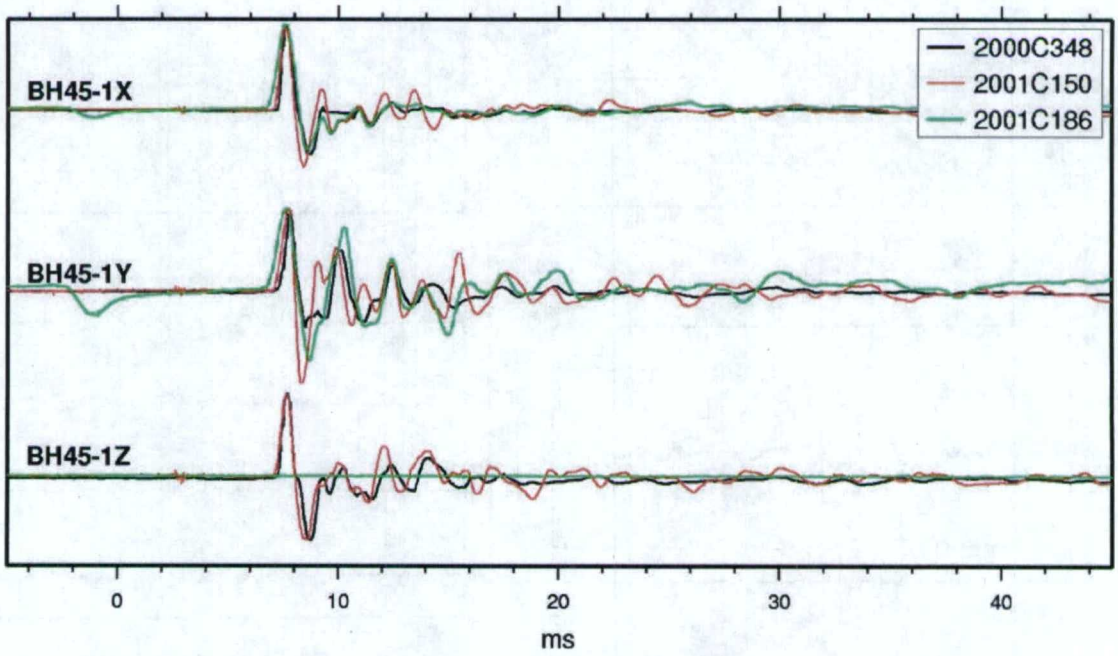

Figure 22. Comparison of the three explosions recorded at the closest borehole (BH45-1). The individual traces have been lowpass filtered, and are scaled by peak value and roughly aligned on the first arrival. Note that the vertical (Z) channel for 2001C186 is defective.

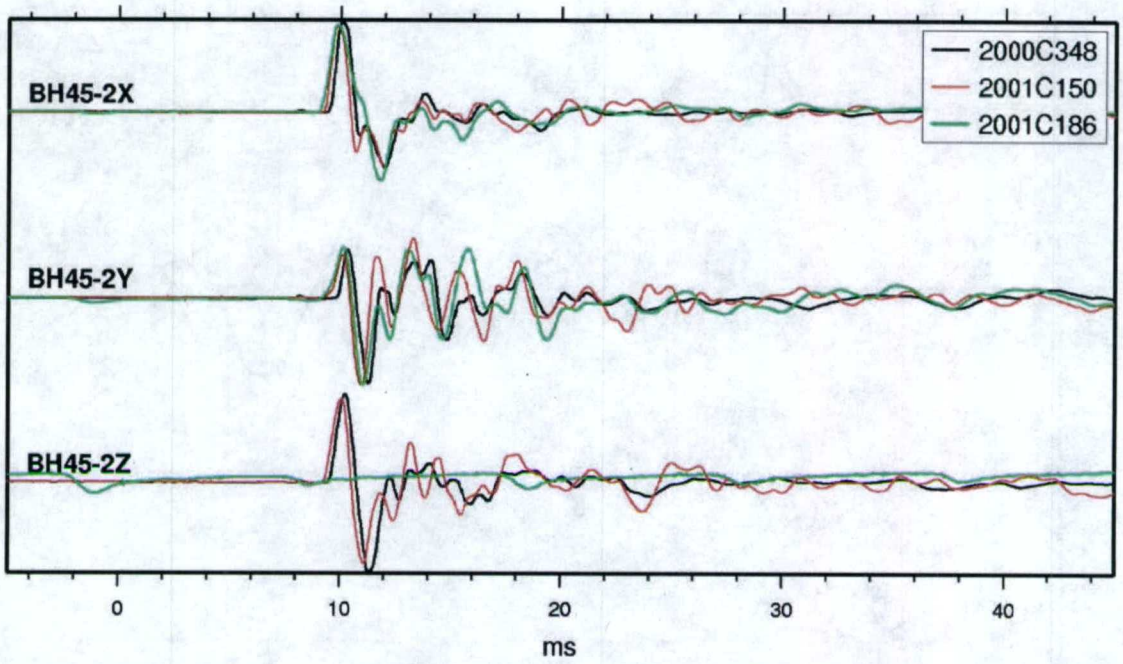

Figure 23. As Figure 22, but for the borehole located 23 m west of the chamber edge (BH45-2). The vertical (Z) channel for 2001C186 is defective also here.

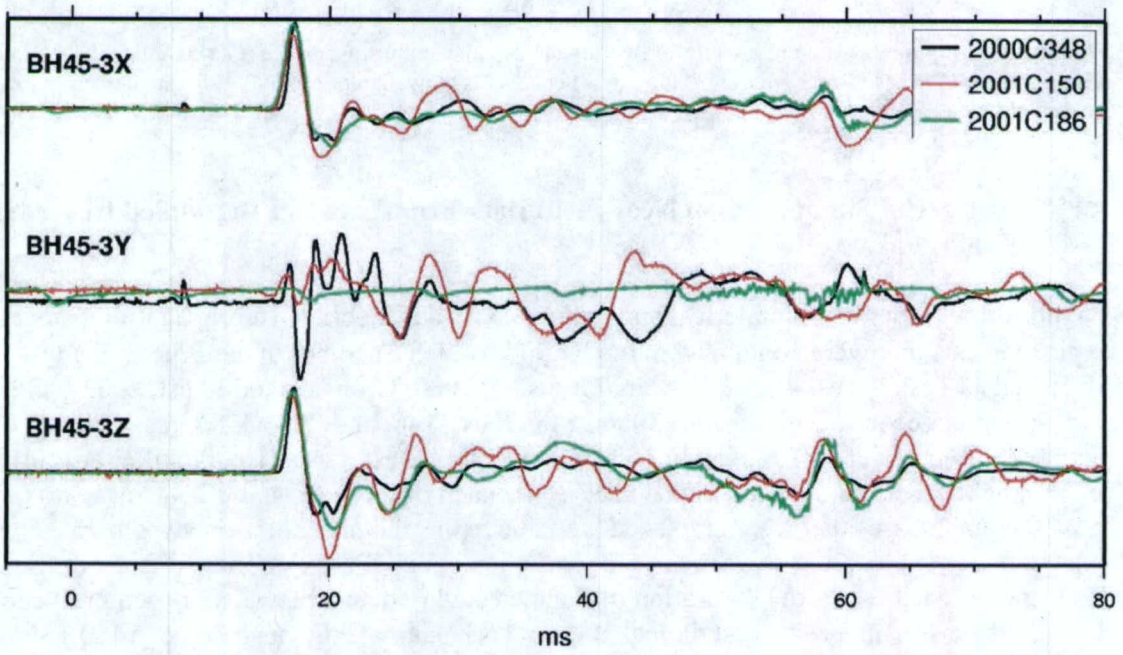

Figure 24. As Figure 22 and Figure 23, but for the borehole located 45 m west of chamber wall (BH45-3). The transverse (Y) channel is defective for the 2001C186 explosion.

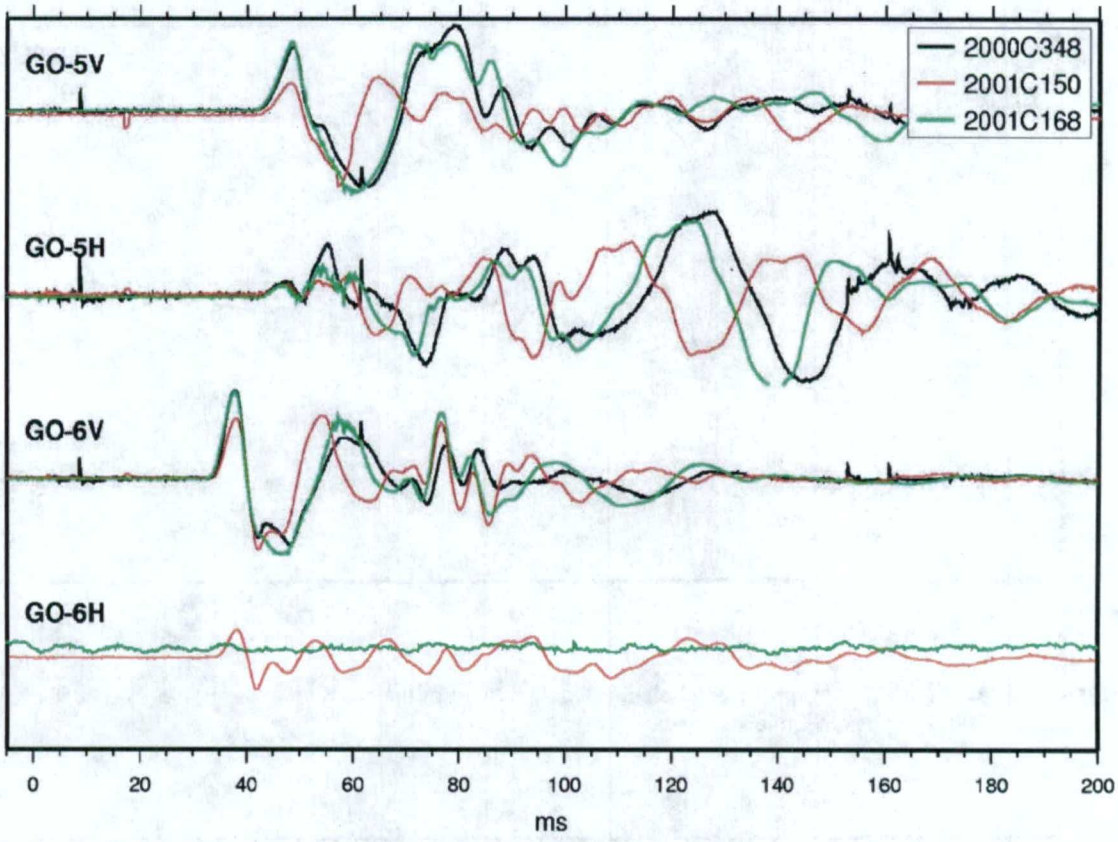

Figure 25. As Figure 22 – Figure 24, but for instruments located at the soil surface (GO-5) and soil-rock interface (GO-6). The GO-6H (soil-rock interface, horizontal) channel is unavailable for 2000C348 and defective for 2001C186.

3.4 Numerical Simulations of Near Field Data From Swedish Decoupled Chamber Explosions

We performed a series of numerical simulations to model shock wave propagation from the three explosive tests that were conducted in the large Älvdalen chamber in hard rock. The tests are identified as Test 3, Test 4a and Test 4b (Grønsten, 2000, Grønsten and Krest, 2002), and correspond to decoupled explosions 2000C348, 2001C150, and 2001C186, respectively. The chamber volume was approximately 1000 cubic meters. Test 3 used 10,000 kilograms (10 tons) of TNT, while Test 4a used 2.5 tons of TNT. For each of these tests, the TNT mass was divided into 10 equal masses that were emplaced well above the chamber floor on styrofoam. The axisymmetric explosive emplacement (about the long axis of the chamber) was in two rows of 5 TNT masses each, with row separation of 5 meters and 6 meters between the center of each of the charge masses in a row. Test 4b had 10 tons TNT equivalent, consisting of 1450 155-mm shells emplaced similarly to the earlier tests in 10 clusters of 145 shells each.

Three-dimensional accelerometers, placed in vertical holes drilled from the surface, were used to record the near field motions from the explosions. We generated particle velocity records by time-integrating these accelerometer records. In the following sections we describe two sets of

calculations: spherically symmetric finite difference calculations for an equivalent volume sphere in granite, and 3D finite difference calculations in which we model the known cavity geometry and layout of explosive in the chamber. In these calculations we model the chamber as sealed at the time of each explosion so that all explosive materials stay in the chamber. However, air pressure measurements at various places in the tunnel complex confirm that, in fact, the chamber was not sealed.

3.4.1 Test Geometry

Test chamber dimensions are roughly 8 meters in width, 4 meters in height, and 30 meters in length. The long axis of this chamber, the parallel direction in the original data reports (our x axis), is in the E-W direction, i.e., in the plane of the three grouted, vertical drill holes containing the accelerometers. This vertical x-z plane (the z axis points upward) is presumed to intersect the center of the chamber, providing a theoretical plane of symmetry since the TNT was emplaced symmetrically about the long axis of the chamber. Thus, the predominant motions at the gauge locations should be in the positive x and z directions, with little motion expected in the horizontal N-S (our y) direction.

The three accelerometer packages are located along a line in this vertical plane of symmetry at an angle of 45 degrees to the vertical. This line does not go through the center of the chamber. Thus, the (spherical) radial direction for our 1D calculations is not along the axis of the three accelerometers. These three gauges, designated as V1, V2, and V3, are at slant ranges (radial distances) of 27.7, 43.1, and 74.4 meters respectively from the center of the chamber. The coordinates of these gauges relative to the center of the chamber (xc and zc) and relative to the closest edge, the top for the z coordinate (xe and ze), are given in Table 3.

Table 3. Coordinates of gauges V1, V2, and V3 relative to center (xc, zc) and closest edge (xe, ze) of the explosion chamber for Tests 3, 4a, and 4b.

Gauge #	Slant range from center (m)	xc (m)	zc (m)	xe (m)	ze (m)
V1	27.7	26.1	9.3	11.0	7.6
V2	43.1	37.7	20.9	22.6	19.2
V3	74.4	60.3	43.5	45.2	41.8

3.4.2 Data Analysis

The accelerometer measurements (and integrated particle velocities) are obtained in the x, y, z, coordinate system defined above. From the raw data figures, we have compiled a table of results for the first signal at each gauge location. For many of the results in Table 4, comparisons between the three explosions appear to be at least qualitatively in line with expectations. Lower peak velocities at the gauges for Test 4a compared with Test 3 are consistent with the more decoupled explosion. The lower peaks for Test 4b, for the same mass of explosive as Test 3, could be due to a lower energy content than expected in the ammunition or a slower detonation compared with the pure TNT detonated in Test 3. Test 4b does give higher peaks than the more decoupled Test 4a.

Table 4. Values of arrival time, time of first peak velocity, rise time, and peak particle velocity components for Tests 3, 4a, and 4b in 1000 m^3 chamber. Times for y component are shown in parentheses if different from other components.

Test # Gauge #	Arrival time of first signal (ms)	Time of first peak (ms)	Rise time to peak (ms)	Peak of x component (cm/s)	Peak of z component (cm/s)	Peak of y component (cm/s)
Test 3 10 tons TNT						
V1	3.4	4.1(4.3)	0.7	41.5	22	16.4
V2	5.7(6.0)	6.8	1.1	12	10.8	3.1
V3	12	13.8	1.8	9.4	3.5	-0.64
Test 4a 2.5 tons TNT						
V1	7.2	8.0	0.8	10	4.8	4.2
V2	9.5	10.4	0.9	2.7	2.2	0.7
V3	16.1	18.1	2.0	1.5	0.4	0
Test 4b 10 tons Ammo						
V1	7.9	9.2	1.3	21.5	defective	7.2
V2	10.1	12.1	2.0	8.1	defective	1.5
V3	16.9	19.4	2.5	5.7	2.3	defective

Note that the y component of the peak particle velocity, expected to be negligible because of the plane of symmetry of the experiment, is a significant fraction of the x and z velocity components, particularly at gauges V1 and V2. This could indicate that the individual drill holes from the surface were not aligned correctly. The y velocity components from Test 3 are less likely to be the result of asymmetric explosive detonation, since the direction of this y motion has changed between gauges. For Test 4b, the vertical channels at V1, V2, and the transverse channel at V3, all became defective for this July, 2001 explosion. Therefore, these defective records are all excluded in the following discussions. The other components for Test 4b are smaller than expected based on comparable yield of Test 4a. This is likely due to the difference in yield efficiency of the ammunition shells used in Test 4b vs. the TNT used in the other tests. The regional signals were also smaller for Test 4b than for Test 4a.

The arrivals for the 10-ton ammunition Test 4b are roughly the same as for the smaller event. One question to be asked is whether the first test damaged the surrounding rock, thus reducing the wave speed. The measured rise times of Test 4a, statistically the same as for Test 3, imply that the rock has not been damaged significantly. The larger rise times for Test 4b may be due to a more diffusive ammunition detonation. The later arrivals for this test may also be linked to the use of ammunition rather than pure TNT.

Table 5 shows the apparent P-wave velocities calculated between individual gauges from the arrival time information and the distance between gauges. These apparent wave speeds do not show any statistically significant decreases due to the earlier shots, particularly near the chamber, where the most damage to the rock would be expected. The large apparent wave speeds in the first (relatively short) segment may be an aberration, since the chamber is clearly neither a point source nor a spherical source and the most direct ray from the center of the long, explosive-filled chamber to gauge V2 does not lie along the ray from the chamber to gauge V1.

Table 5. Apparent P-wave velocities calculated between individual gauges for Tests 3, 4a, and 4b.

Test #		3	4a	4b
Segment	Segment length (m)	P-wave speed (m/s)	P-wave speed (m/s)	P-wave speed (m/s)
V1-V2	16.41	7133	7132	7457
V2-V3	31.96	5073	4842	4700
V1-V3	48.37	5624	5641	5374

The discussions so far have dealt with the first signals only. Some description of the differences between test results for the longer term signals follows. For Test 3, a slow rise in particle velocity is measured at gauge V1, beginning about 30 ms and peaking at about 200 ms with a magnitude of 30 cm/s, about 75% of the first peak. This second signal is not seen at the two other gauges for Test 3. For Test 4a, a similar second signal begins at gauge V1 at 130 ms, peaks at 270 ms with a magnitude of 17 cm/s, much larger than the first peak. Again this signal is not seen on the other two gauges. Thus, this signal is unlikely to be due to any interaction with the free surface, located approximately 100 meters above the chamber. For Test 4b, a large second signal is seen on all three gauges, with a magnitude of 12 cm/s at V1, 9 cm/s at V2, and 6 cm/s at V3. Detailed two-dimensional calculations will be needed to understand these later time measurements.

For comparison with spherically symmetric one-dimensional calculations to be discussed below (we ignore the free surface effect), we rotated the measured values of the x and z components of the particle velocities about the line from the center of the test chamber to the gauge to obtain the radial and tangential (in-plane) components, i.e., to cylindrical, rather than spherical, components. The recorded y components of the acceleration (and particle velocities) were thus treated here as a measure of unexpected large asymmetries in the results of a theoretically axisymmetric experiment.

These asymmetric accelerometer measurements are not yet understood. Possible explanations include inhomogeneities in the surrounding rock, the precision of the axisymmetric gauge emplacements, and/or the symmetry of the explosion emplacements or detonations. We believe that the explosive gases venting from the chamber into the tunnel complex, while certainly an asymmetric effect, would not strongly effect first arrivals and peaks at the three accelerometers.

Table 6 shows the rotated peak values of the in-plane radial (r) and tangential (t) velocity components together with the y component and the magnitude of the peak velocity vector for Tests 3, 4a, and 4b. In general, the radial peak velocities are only slightly smaller than the peak velocity magnitudes. We note again that for Test 4b only, gauges V1 and V2 have defective z-channels and V3 has defective a y-channel. Thus, only t and r components are computed at V3.

Table 6. Values of in-plane radial, r, in-plane tangential, t, and y components of peak particle velocity for Tests 3, 4a, and 4b in 1000 m^3 chamber. Positive t velocity is counterclockwise from (upward) direction.

Test # Gauge #	Peak of r component (cm/s)	Peak of t component (cm/s)	Peak of y component (cm/s)	Magnitude of peak velocity (cm/s)
Test 3 10 tons TNT				
V1	46.5	-7	16.4	49.8
V2	15.6	-3.9	3.1	16.4
V3	9.7	2.7	-0.64	10.1
Test 4a 2.5 tons TNT				
V1	11	-1.2	4.2	11.8
V2	3.5	-0.7	0.7	3.6
V3	1.7	0.3	0	1.7
Test 4b 10 tons Ammo				
V1	N/A	N/A	7.2	N/A
V2	N/A	N/A	1.5	N/A
V3	6.0	1.5	N/A	N/A

N/A indicates defective channels involved

In the absence of the large, unexpected y components, the values of the in-plane tangential component of peak velocity may be considered a measure of the physical effect of the non-sphericity of the test chamber and explosive emplacement. Using a point source argument, this non-spherical effect would be expected to be largest for the closest gauge, V1, and smallest for the furthest gauge from the chamber, V3. In fact, the Table 4 shows substantial tangential, t, components for all working gauges (10% or more of the radial component). At gauge V3 for all three tests, the tangential velocity is positive (counterclockwise from the upward direction), while at gauges V1 and V2 for Tests 3 and 4a, the tangential velocity is clockwise. We do not understand this change in direction of the tangential velocity. Note however that the magnitude of peak in-plane tangential motion, in many cases, is quite similar to the peak y component.

3.4.3 Spherically Symmetric Calculations

As a first step toward understanding these near field velocity measurements, we performed spherically symmetric simulations for Tests 3 and 4a and compared the results with the observations. In these finite difference calculations, the long test chamber and axisymmetric explosive configurations were approximated as a spherical mass of TNT centered in a 1000 cubic meter spherical chamber of approximately 6.20 m. For Test 3, the 10,000 kg (10 metric tons) of TNT gave an outer radius of ~1.136 meters for the TNT, assuming normal TNT density of 1.63 g/cm^3. For Test 4a, the radius of the 2.5 ton TNT sphere was calculated to be ~0.7155 m.

The explosive was center detonated, with the propagation of the detonation wave through the TNT computed using the JWL equation of state. The JWL equation of state has been used to accurately describe the pressure-volume-energy behavior of the detonation products of explosive in metal acceleration applications. The equation is (Lee et al., 1973)

$$P = A(1-\frac{\omega}{R_1 V})e^{-R_1 V} + B(1-\frac{\omega}{R_2 V})e^{-R_2 V} + \frac{\omega E}{V}$$

where P=pressure in Mb, E=energy density in Mb-cc/cc and V= (volume of detonation products)/(volume undetonated explosive). For pure TNT, the parameters are listed in Table 7.

Table 7. The experimental values for pure TNT parameters in the JWL equation.

Parameter	Value	Unit conversion
A	3.712 MB	$3.712\times10^{12}\,dyn/cm^2$
B	0.03231 MB	$3.231\times10^{10}\,dyn/cm^2$
C	0.01045 MB	$1.045\times10^{10}\,dyn/cm^2$
R1	4.15	
R2	0.95	
ω	0.30	

The surrounding air was modeled using an equation of state for air originally developed by the Air Force Weapons Laboratory, which has subsequently been validated through many successful simulations at SAIC. The rock surrounding the test chamber was modeled as granite.

For the simulations shown here, a relatively simple model was used to describe the rock behavior. This granite model (YF-AF, Stevens et al., 2003) presumed an elastic response coupled to a non-associated radial return flow rule with a failure surface based on that measured in the laboratory on fractured granite cores from the Piledriver test site. Elastic constants used were a bulk modulus of 483 kb, a shear modulus of 207 kb, and a density of 2.60 g/cm^3.

Figure 26 shows the radial particle velocities calculated at the radial ranges of the three gauge locations (V1, V2, and V3) from Tests 3 and 4a. The dashed particle velocities are the gauge measurements rotated into the in-plane radial direction as discussed above. Comparisons between simulated and measured particle velocities in the first signals, except for the arrival times, are fairly good. Note that the calculated subsequent signals represent reverberations in a spherical cavity and should not be expected to agree well with the measurements from these tests in a long chamber.

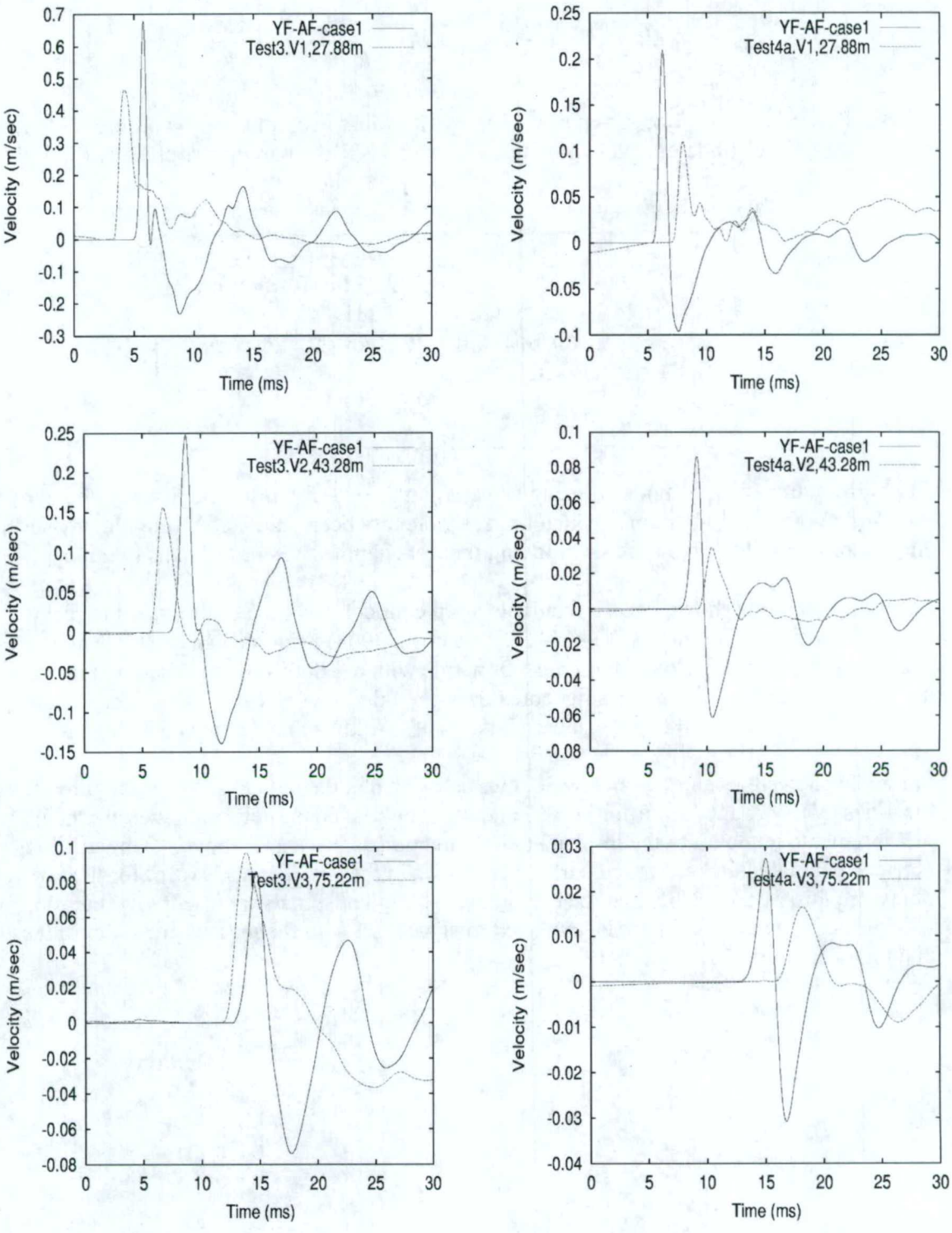

Figure 26. Radial particle velocities from a spherically symmetric simulation of Test 3 (10tons, left) and Test 4a (2.5 tons, right). Measurements at gauges V1, V2, and V3 are shown as dashed lines.

Figure 27 shows the velocity data and spherical calculation scaled to correspond approximately to the same yield. Using cube root scaling, increasing the yield by a factor of four leads to the same waveforms with all dimensions and the time scale increased by a factor of $4^{1/3}$. So the velocity waveform from a 2.5 ton explosion recorded at a distance of gauge V1 (27.7 m) and the time scale increased by that factor should be approximately the same as the velocity waveform from the 10 ton explosion at the distance of gauge V2 (43.1 m). Scaling does not work exactly because the chamber volume remains the same in the two cases. Nevertheless, it is useful for comparison. Figure 27 shows that both the data and the calculation for the 10 ton case are somewhat larger than the scaled 2.5 ton case, consistent with some modest increase in coupling due to nonlinear deformation from the larger explosion. The calculated waveforms at this location are larger than the observations. As discussed in the following section on 3D calculations, this is due to the location of the gauges off the long end of the chamber.

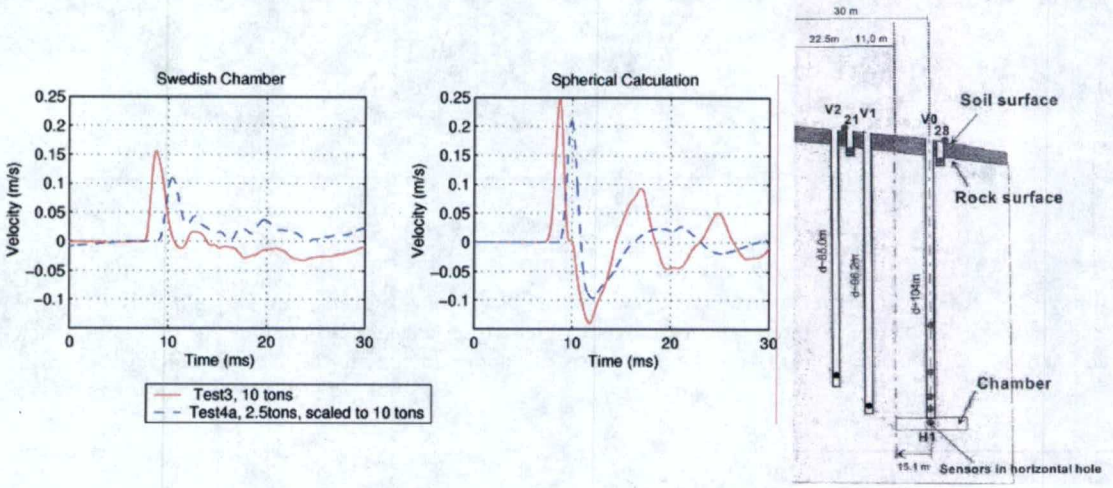

Figure 27. Red lines show the 10 ton chamber data and the spherical calculation at gauge V2. Blue lines show the 2.5 ton data and calculation at gauge V1, scaled to 10 tons (by increasing time scale by $4^{1/3}$) which is approximately equivalent to recording at V2. Coupling predicted from the spherical calculation is larger than the data at this location. The geometry of the gauges is shown on the right.

Figure 28 shows a comparison between the "observed" chemical decoupling factors for the Swedish explosions and decoupling factors for a series of calculations of chemical explosions in a cavity in granite. "Observed" is in quotes because we do not have data from a tamped explosion for comparison. Instead, we scaled the decoupling factor of the most decoupled explosion to 100 to agree with the calculation for a fully decoupled explosion. As noted before, the larger chamber appears to decouple better than the smaller chambers for the same charge density. The figure shows that the explosions remain almost fully decoupled until the charge/volume is approximately equal to 10, after which increases in yield cause a rapid decrease in decoupling. The calculation also shows this effect of nearly constant decoupling followed by a rapid decline. In the calculation the decline occurs at a higher charge/volume, most likely because the Swedish cavities are not spherical, which increases coupling. We investigate this further with 3D calculations in the next section of this report.

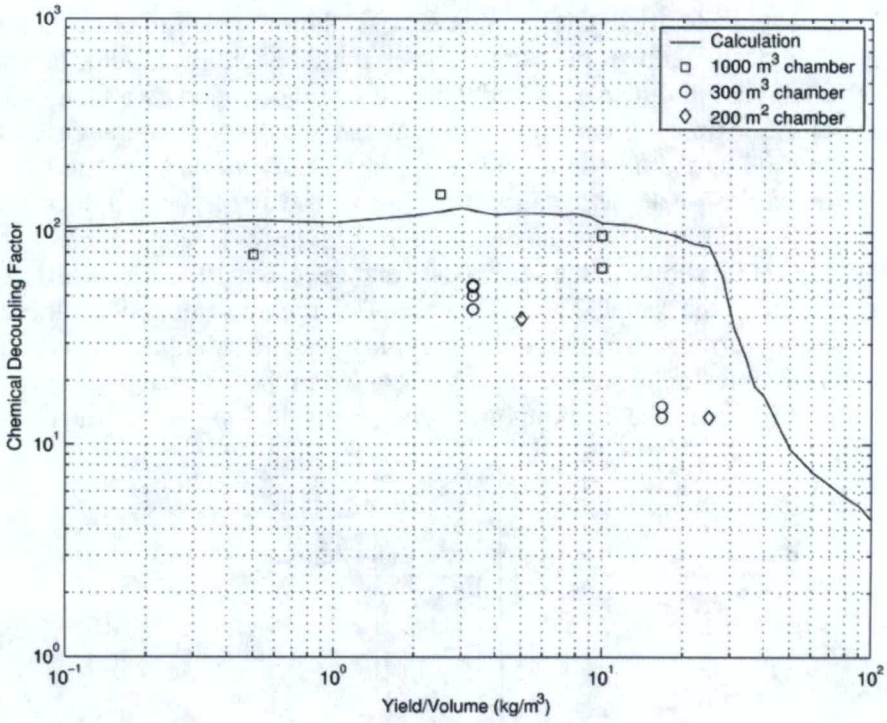

Figure 28. Observed and predicted chemical decoupling factor for Swedish chamber explosions. Calculations were for a chemical explosion in a 6.3 meter spherical cavity in hard (non-weakening) granite. The decoupling factor contains an unknown scale factor. The horizontal axis corresponds approximately to the overdrive factor above full decoupling.

3.4.4 Three-Dimensional Calculations

In order to increase our understanding of the Swedish chamber explosions, several three-dimensional finite difference calculations were performed using the "Stellar" code. Stellar is a second-order accurate Eulerian two- and three-dimensional stress wave propagation code with the same constitutive models that were used for the spherically symmetric calculations. The chamber was modeled as an air-filled chamber with dimensions 4.8m high (x axis), 30m long (y axis), and 7.2m wide (z axis). The near field results are sensitive to the layout of the explosive in the chamber, so several layouts were used in the simulations. The grid is shown in Figure 29. All calculations were performed in a 1/8 space, taking advantage of symmetry across the three planes through the center of the rectangular chamber. In this first calculation, the finite difference grid was 20m x 30m x 20m in size, with 100x100x100 grid blocks. The chamber is 2.4m x 15m x 3.6m. The explosive was placed in a flat layer along the x=0 plane, with a dimension of 0.2m x 2.7m x 0.8m, with a total energy of 1.25 tons. Note that because of symmetry, all linear dimensions are effectively multiplied by two and volumes by eight, so this is equivalent to a 10 ton explosion in the chamber described earlier.

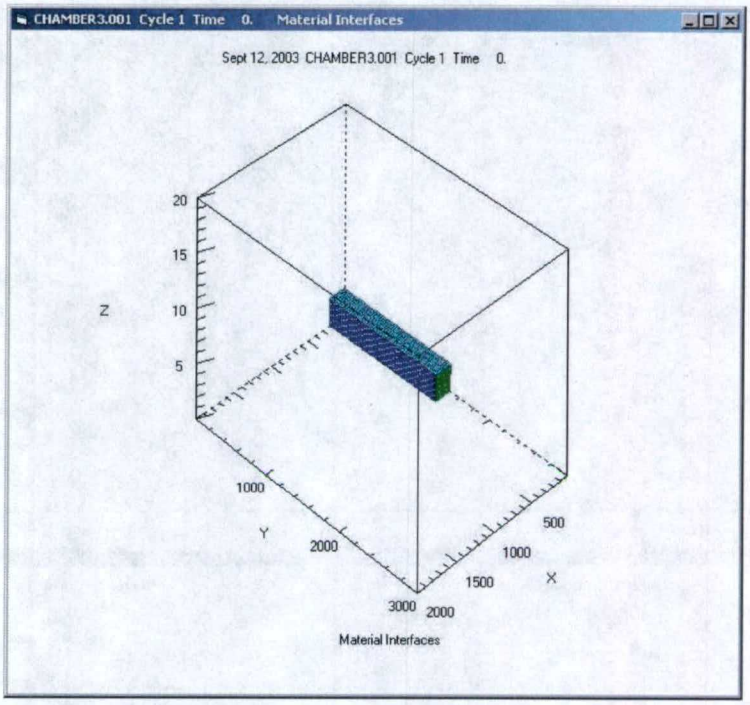

Figure 29. Geometry of grid used in one of the 3D calculations. The rectangle in the center is the chamber. There is symmetry about all three axes. Units of X, Y axes are in cm, Z is in meters.

The series of images in Figure 30 shows the evolution of the pressure field in the x-y plane near z=0 as a function of time in the calculation. The images show the initial high pressure field immediately after detonation, the propagation of the shock into the surrounding chamber wall, the propagation of the wave down the long axis of the chamber, a secondary high pressure region as the shock hits the end of the chamber, and initiation of the pressure wave that propagates out of the nonlinear region that later becomes visible as a seismic signal. The region closest to the explosion is hit hardest and a residual pressure due to nonlinear deformation remains both here and at the end of the chamber. A second calculation was performed with the same geometry, except that the explosive was reduced to an area of 0.2m x 2.7m x 0.2m, corresponding to a total energy (including symmetric regions) of 2.5 tons. Figure 31 shows a comparison of the regions of nonlinear deformation for these two calculations.

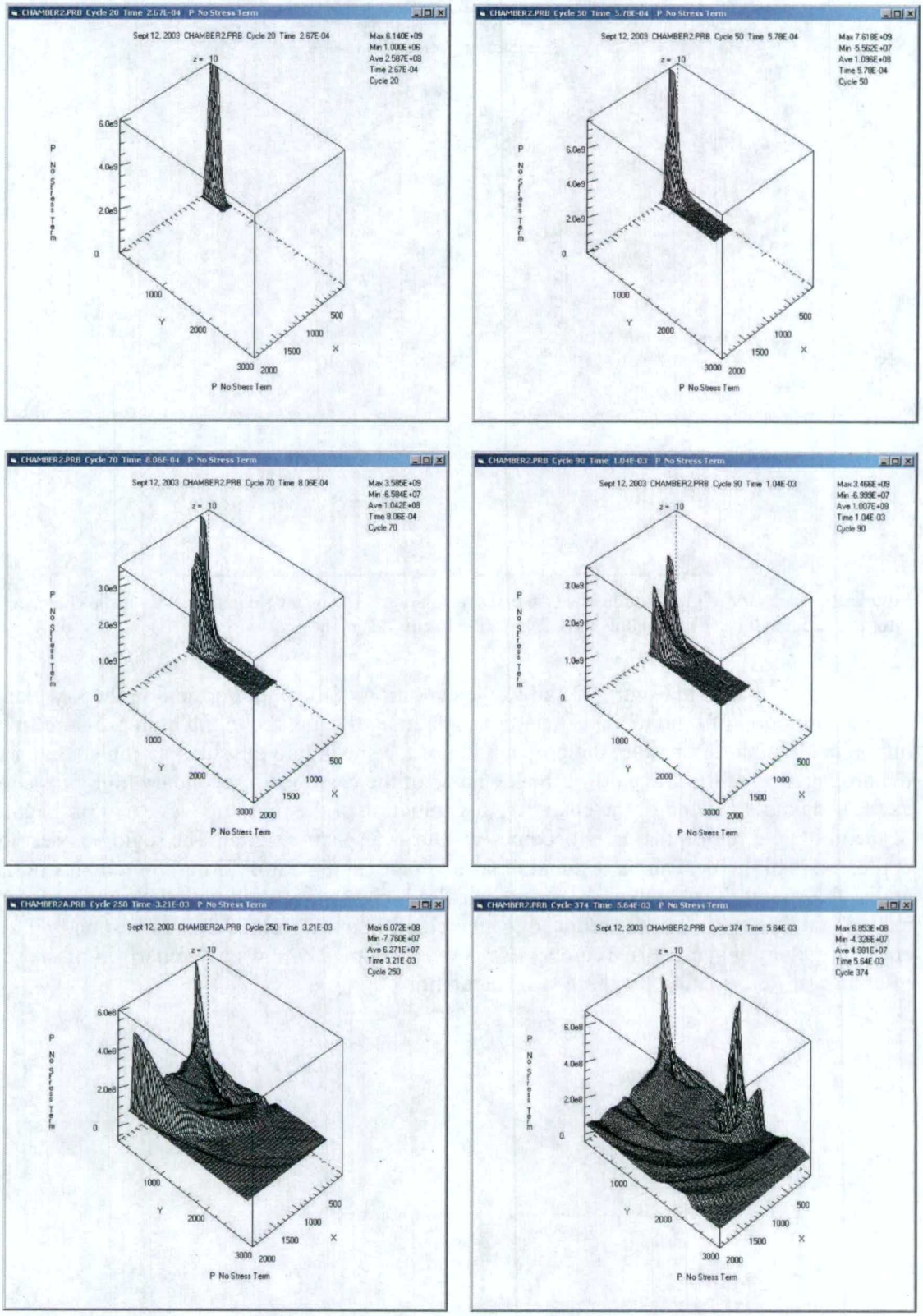

Figure 30. Pressure from 3D chamber calculation at times of 0.27, 0.58, 0.8, 1.0, 3.2 and 5.6 msec.

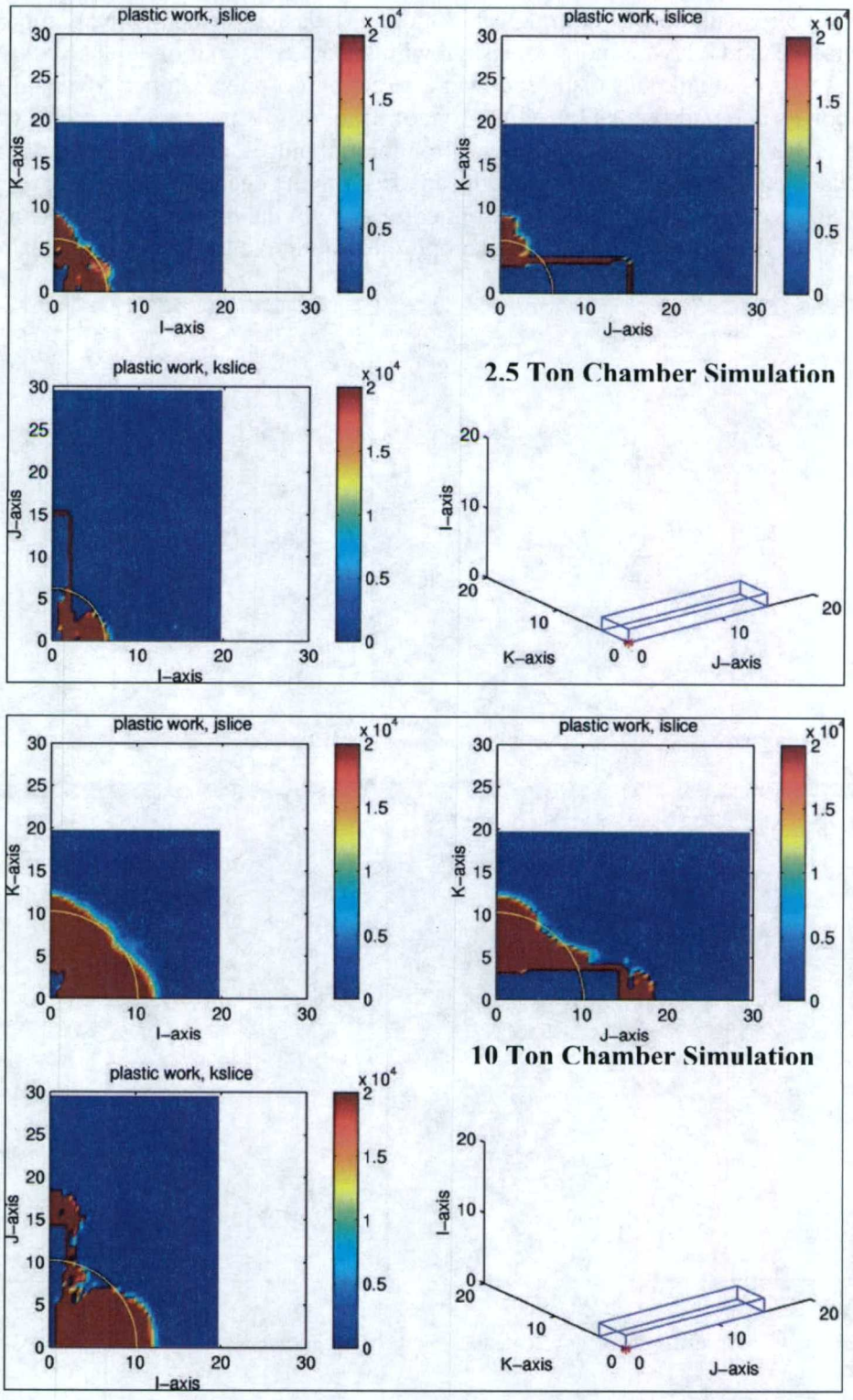

Figure 31. Regions of nonlinear deformation for 2.5 ton chamber calculation (top) and the 10 ton chamber calculation (bottom). The three figures show the nonlinear deformation around each of the three axes. The yellow line is the region of nonlinear deformation for an equivalent volume sphere.

A third set of calculations (Figure 32 and Figure 33) was performed with an improved model for the explosive, and a layout more consistent with the actual layout of explosives, which was set out in a series of small pads dispersed over a larger part of the chamber. We model this in the simulation as two pads which by symmetry corresponds to 8 pads each of twice the thickness used in the calculation. The result is two strong initial pulses, and a more complicated state within the chamber, but a somewhat reduced effect on the chamber wall. Note also the radiation pattern of the outgoing wave, with a stronger pressure in the direction along the narrowest dimension of the chamber, and reduced amplitudes along the long axis of the chamber.

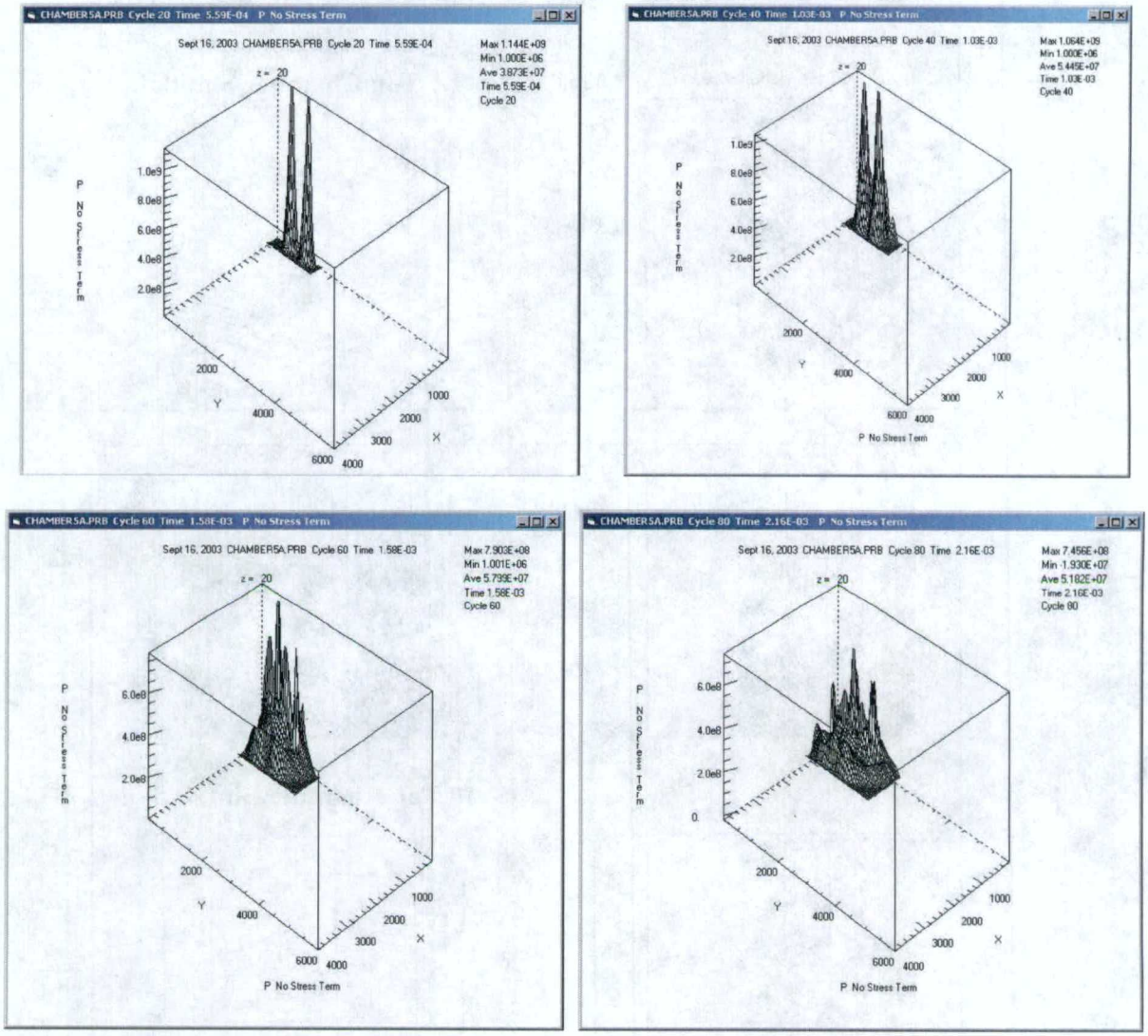

Figure 32. Pressure from 3D chamber calculation with better explosive representation at times of 0.6, 1.0, 1.6, and 2.2 msec.

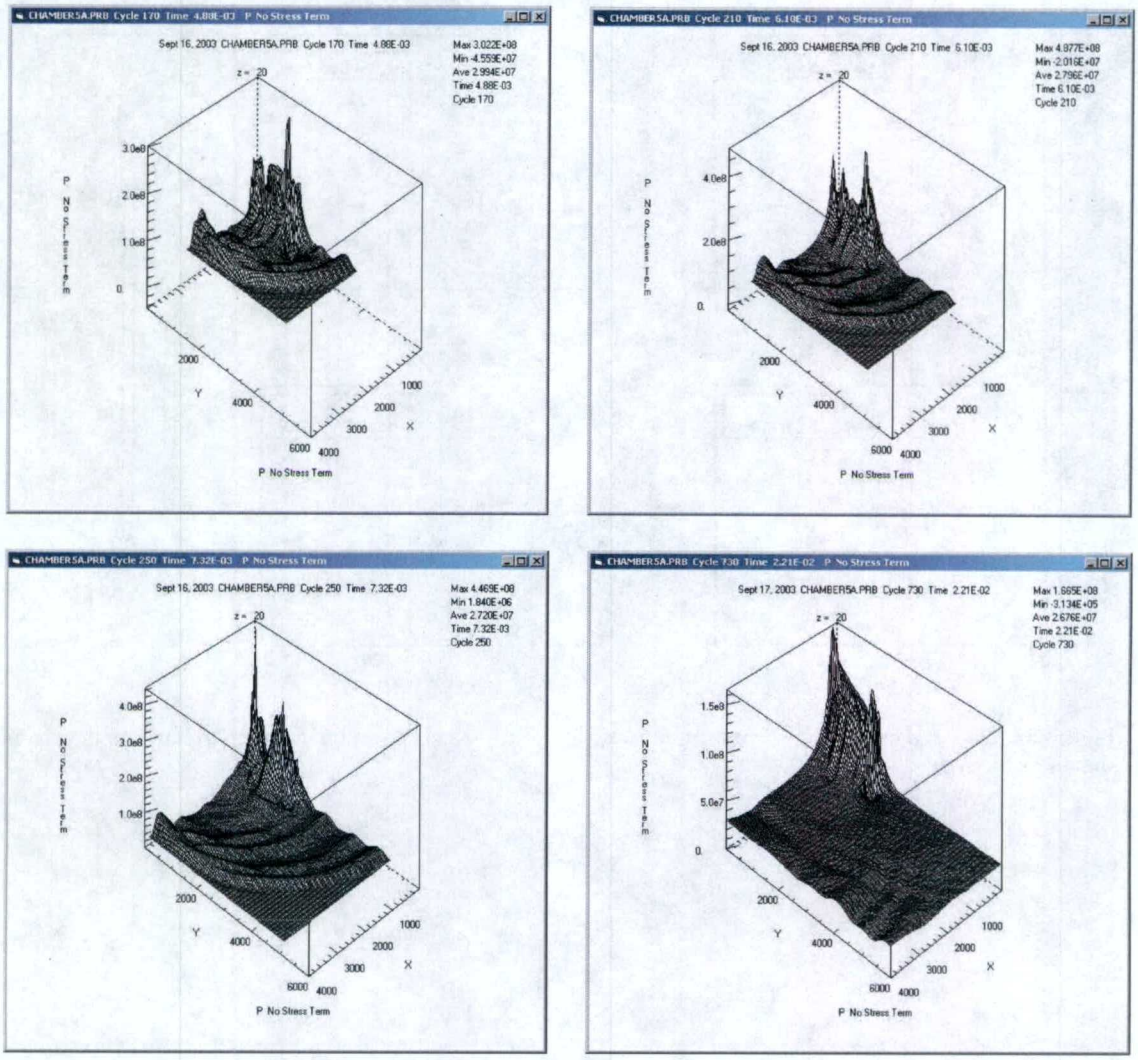

Figure 33. Pressure from 3D chamber calculation with better explosive representation at times of 4.9. 6.1, 7.3 and 22 msec.

Figure 34 shows that calculated waveforms at the locations of recording stations V1 and V2, together with the horizontal and vertical components of the recorded waveforms at the same locations. As with the spherical calculations, the chamber reverberations are stronger than the observations, however the peak amplitudes and general shape and duration of the waveforms are reproduced fairly well. As noted above, there is a strong radiation pattern to the waveforms, with stronger amplitudes above and below the chamber and reduced amplitudes along the long axis of the chamber near the recording points V1 and V2.

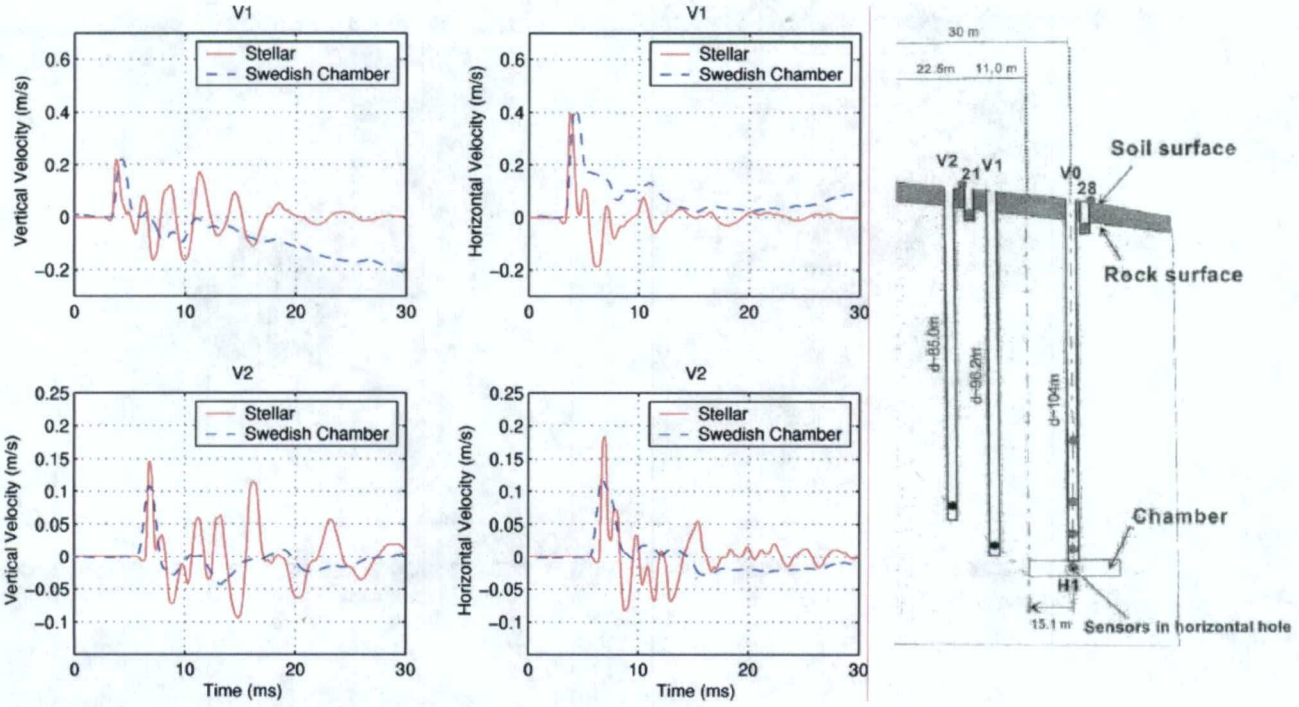

Figure 34. Data and calculated waveforms at stations V1 and V2. The station geometry relative to the chamber is shown on the right.

4 KIRGHIZIA DECOUPLED CHEMICAL EXPLOSIONS

During the summer of 1960, Soviet scientists carried out a series of HE cavity decoupling tests in a mine in the Tywya Mountains of Kirghizia. This program included tests designed to evaluate the effects of cavity shape and charge geometry on decoupling effectiveness, in addition to conventional spherical cavity tests similar to those employed in the corresponding U.S. COWBOY test series. The Kirghizia test series was composed of 10 tamped and 12 decoupled explosions with yields of 0.1, 1.0 and 6.0 tons. For the cavity tests the explosives were suspended in the chambers and included cases in which the explosives were positioned off center, near the cavity walls. The configurations of the various cavity tests are graphically summarized in Figure 35 for each of the five test chambers.

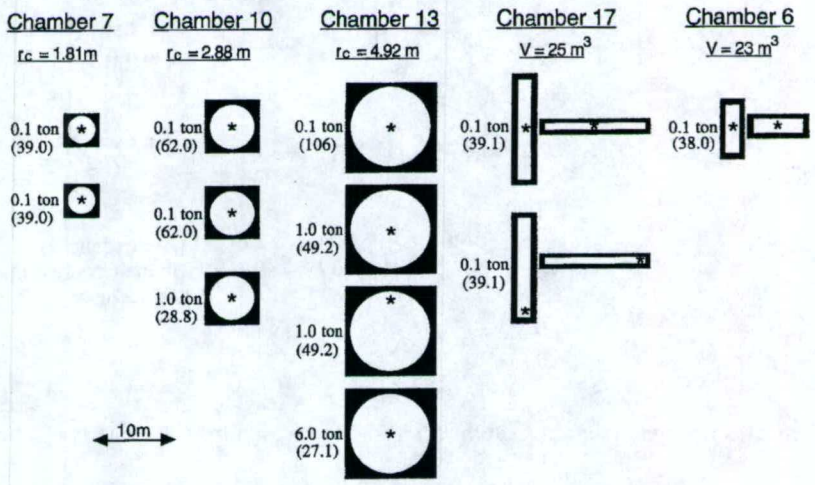

Figure 35. Graphical summary of the Kirghizia HE decoupling tests conducted in each of the excavated explosion chambers. The asterisk denotes the emplacement location of the charge within the chamber for each test. For the nonspherical cases, both horizontal (left) and vertical (right) sections through the chambers are displayed. The numerical values shown in parentheses below the yield values are the scaled radii in $m/kt^{1/3}$, with equivalent volume spherical cavity values listed for the nonspherical cases.

In our previous analysis of these tests (Murphy et al, 1997), we focused on free-field data recorded in the mine at distances on the order of 10 – 200 m. Unfortunately, only limited waveform data were available from this regime and, consequently, the analyses focused primarily on comparisons of peak amplitude values. While such comparisons provided a reasonable basis for comparing the relative decoupling effectiveness of different cavity configurations, they did not provide an adequate data set for confidently determining the frequency dependence of the absolute level of the decoupling factor. Consequently, under the current effort, we have recovered and digitized seismic data from these tests recorded at surface stations located at distances of 5 and 10 km. High quality recordings are available from the 1 ton tamped and decoupled tests at the 5 km station, and the 6 ton tamped and decoupled tests at the 10 km station. Results of detailed analyses of these data have proven to be generally quite consistent with those obtained from the previous analysis of the corresponding free-field data. Examples of these data are shown in Figure 36 which provides a comparison of vertical component recordings at the 5 km station from 1 ton tamped and decoupled explosions. In this

case, the decoupled tests were conducted at the center of spherical cavities with radii of 4.92 and 2.88 m, and 1 m from the wall of the 4.92 radius cavity. It can be seen that the signal levels for the tests in the centers of the two different sized cavities are very comparable, indicating peak motion decoupling factors of about 20 and suggesting that both of these tests in different size cavities were fully decoupled. The signal level for the test near the cavity wall is about a factor of 2 larger, suggesting some significantly enhanced coupling associated with local nonlinear wall response.

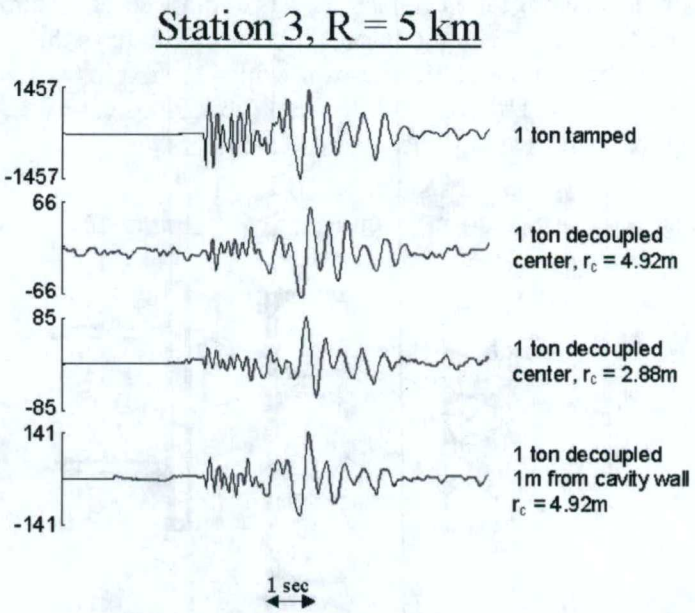

Figure 36. Vertical component recordings at the 5 km surface station from 1 ton tamped and decoupled explosions.

Recordings from the 6 ton tamped and decoupled explosions at the 10 km station are shown in Figure 37. In this case the decoupled explosion was detonated at the center of the 4.92 m radius spherical cavity. Again, the peak signal levels from the two tests shows a chemical decoupling factor of a little more than 20, consistent with the results from the 5 km station and suggesting that this larger test was also fully decoupled . We have computed frequency-dependent chemical decoupling factors between 1 and 4 Hz from these 5 and 10 km station recordings and the results are shown in Figure 38, where it can be seen that the decoupling factors for the two 1 ton tests in the centers of the different sized cavities over this frequency band are essentially identical and consistent with a low frequency chemical decoupling factor in the range 20 - 30. This confirms that these explosions must have been essentially fully decoupled. The frequency dependent chemical decoupling factor for the 1 ton test near the cavity wall is quite similar to the other two in shape, but lower by about a factor of 2, independent of frequency over this range. The results from the 6 ton test are in good agreement with those of the fully decoupled 1 ton tests, suggesting that it also was essentially fully decoupled. The chemical decoupling factor for all of these fully decoupled tests over this frequency band is somewhere in the range of about 20 to 30. Also shown on this figure are the corresponding results at higher frequency (i.e. 10 – 200 Hz) obtained previously by Murphy et al (1997) using the limited free-field waveform data. It can be seen that the results from the two distance regimes are generally quite consistent, confirming a low frequency chemical decoupling factor in the range of 20 – 30 for these fully decoupled tests in limestone.

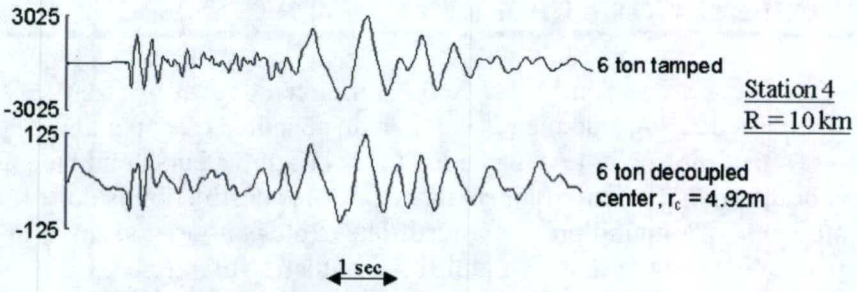

Figure 37. Vertical component recordings from the 6 ton tamped and decoupled tests at the 10 km station.

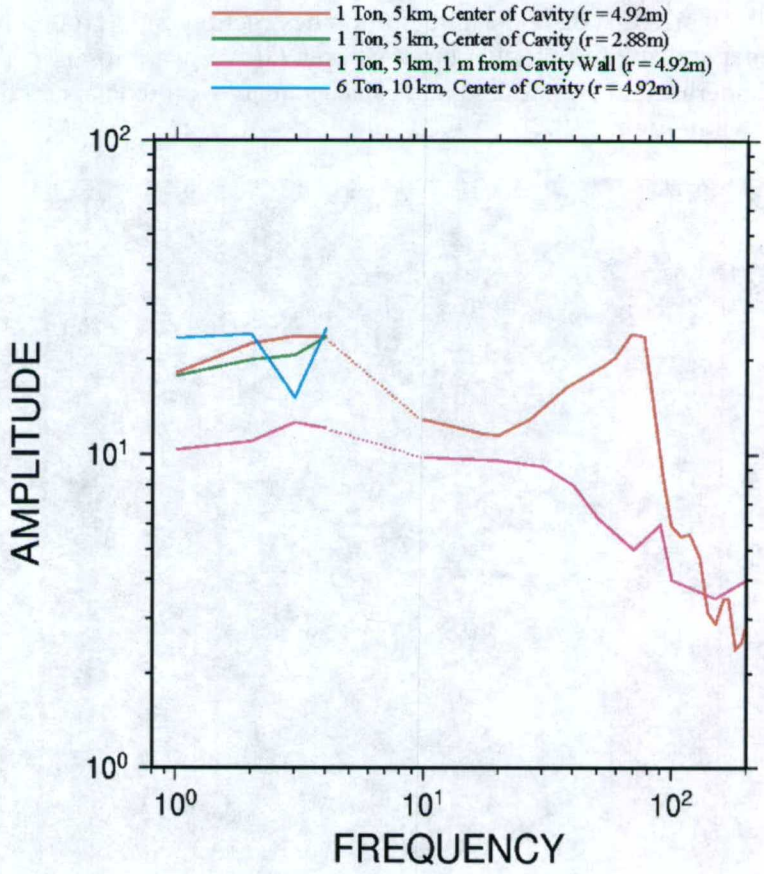

Figure 38. Frequency dependent chemical decoupling factors for the 1 and 6 ton tests at the 5 and 10 km stations. Also shown are the corresponding results at higher frequency (i.e. 10 – 200 Hz) obtained previously by Murphy et al (1997) from the corresponding free-field data.

5 DATA COLLECTION AT LØKKEN GRUVER

Decoupled explosions are regularly carried out at Løkken Gruver by NAMMO-NAD. These explosions take place at 800-900 meters depth in an abandoned copper and sulphur mine. The explosions are small (normally less than 1000 kg TNT equivalents), and the purpose is ammunition destruction. For environmental reasons, this destruction is done in an abandoned mine, and all types of ammunition is involved. The explosions are too small to be detectable on any of the permanent installations in middle and southern Norway.

NAMMO-NAD is affiliated with NAMMO, Nordic Ammunition Company, also dealing with ammunition destruction in Sweden. The company has been in operation for several years, and is one of few in the world that does the ammunition destruction underground in an abandoned mine. The copper and sulphur production in Løkken Gruver was closed in 1984, leaving several kilometers of underground tunnels and open spaces intact with roads and railways. The layout of the mine is shown in Figure 39.

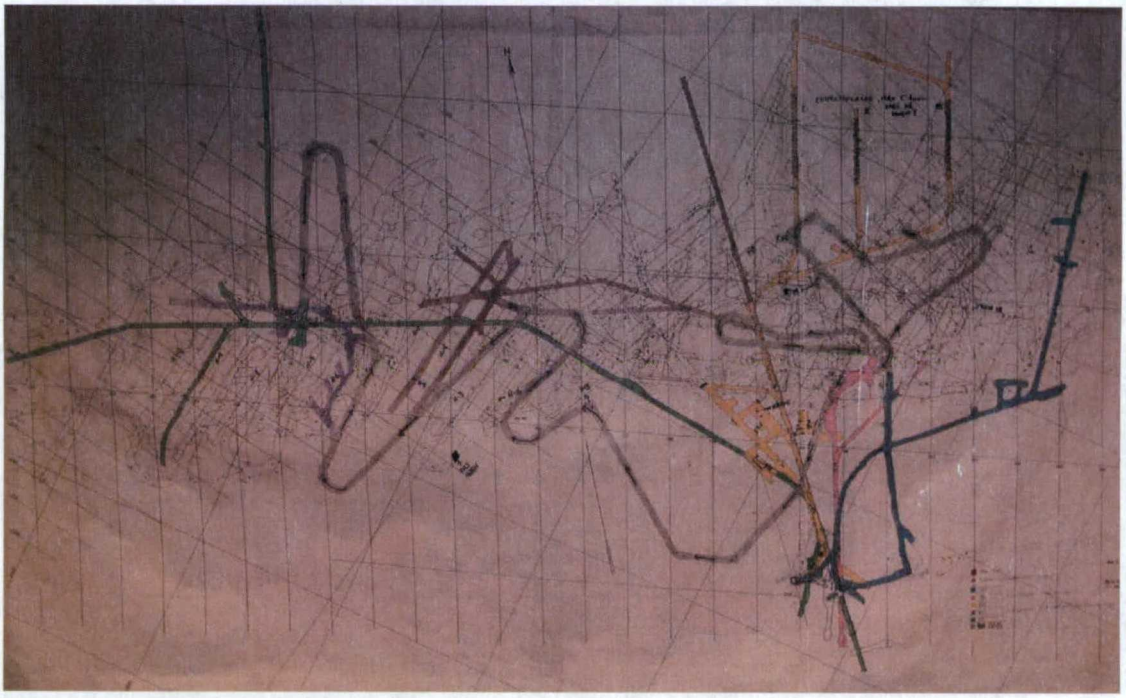

Figure 39. Mine map. Vertical lines indicate 27 meter intervals, however, the accuracy is uncertain. Photo from wall-map.

The present day ammunition destruction covers everything from small shells to bombs and mines, and different explosives (from ammonium-nitrate with a TNT equivalent of around 0.82 (ANFO) to hexotonal with a TNT equivalent of 1.67). The ammunition is typically destroyed in open spaces where fragments do not cause excessive damage to the walls and roof, and with sufficient open voids for a quick decay of the pressure wave. The pressure is released through the tunnels with the normal ventilation system. Explosions are only done once a day (often in groups) so that the air is ventilated until the next working day. The charges at each site are in the range 300 to 1000 kg,

however, two or three sites may be detonated simultaneously (same msec.). The charge bed is gravel sediments (up to 3 meters) and the charges are put on wooden pallets leaving air between the ground and the charge. A typical explosion site configuration is shown in Figure 40.

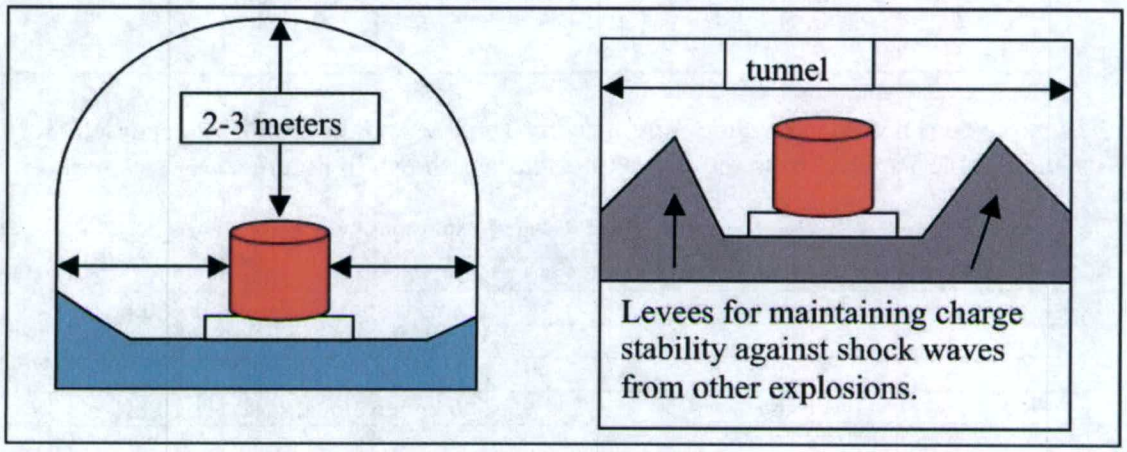

Figure 40. Typical geometry of the tunnels where the charges were detonated. Gray indicates loose gravel sediments.

Three GeoSys instruments were deployed at the locations listed in Table 8 and shown on Figure 41. The explosions were detonated approximately 100-200 meters to the west of the tower marked on the map. The instruments were all deployed on hard rock outcrops.

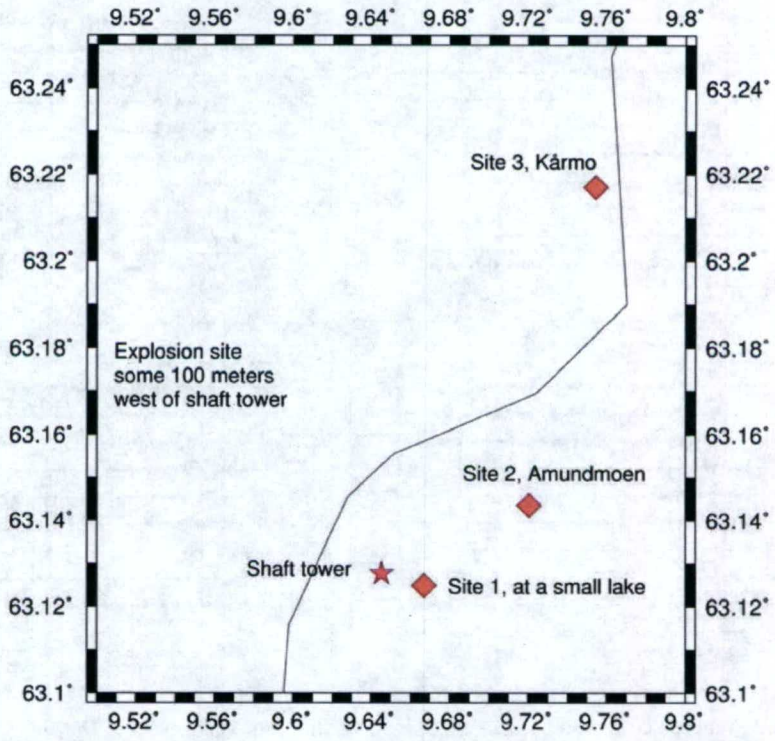

Figure 41. Map of the Løkken recording sites relative to the shaft tower. The gray line is a river.

Table 8. Coordinates of recording sites and shaft tower and distance to shaft tower.

Site	Latitude	Longitude	Elevation(m)	Distance to Tower (km)
Shaft Tower	63.12764	9.64541	290	
Site 1	63.12476	9.66697	296	1.1
Site 2	63.14344	9.72029	189	4.2
Site 3	63.21695	9.75428	69	11.4

The explosions recorded on June 7 are listed in Table 9, and the explosion recorded on June 8 is listed in Table 10. Data from the four explosions are shown in Figure 42.

Table 9. June 7 explosions.

Explosion Number	Site in the Mine	Charges	TNT Equivalent
1 (simultaneous detonation)	913	Six 75 kg bombs	450 kg + 501 kg = 951 kg
	H6	300 kg hexotonal	
2	UO	800 kg mixed types	800 kg
3	UO	600 kg hexotonal	1002 kg

Table 10. June 8 explosion.

Explosion Number	Site in the Mine	Charges	TNT Equivalent
4 (simultaneous detonation)	H6	Four 75 kg bombs	~1000 kg
	H7	Four 75 kg bombs	
	913	400 kg mixed types	

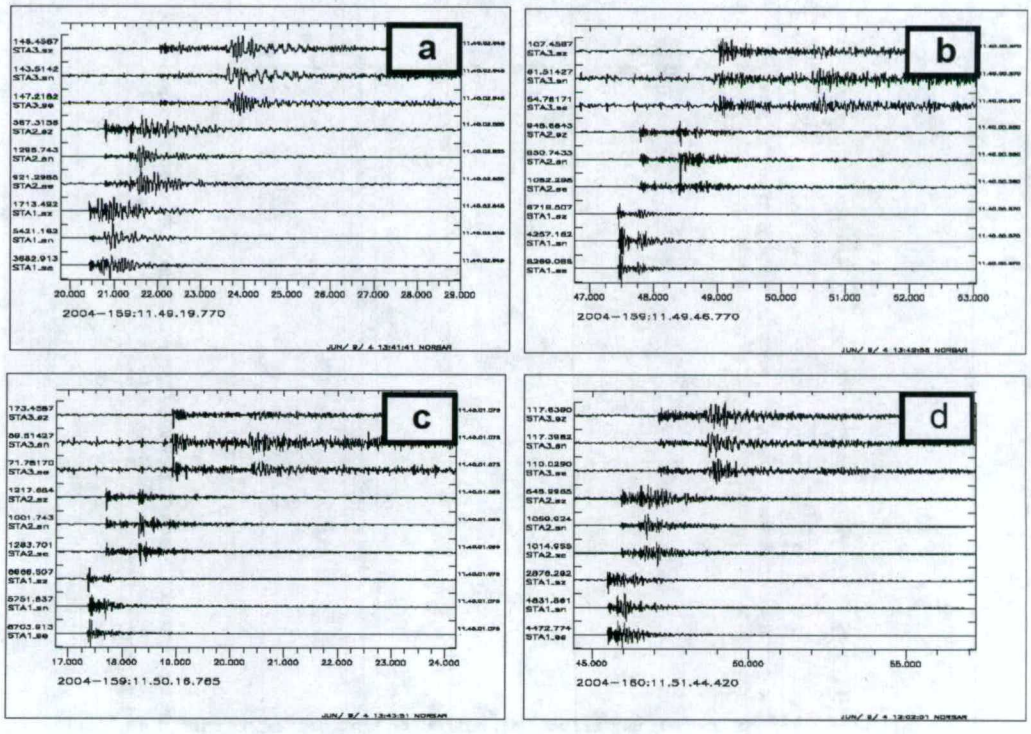

Figure 42. Seismic records collected at Løkken. a, b and c show the records from the June 7 sequence, and d shows the June 8 explosion.

Spectra of the P-phase records from the station at 11.4 km are shown in Figure 43. The instrument response was removed and replaced with the HFS instrument response as was done with the Älvdalen data in Figure 16. Spectral shape is generally the same. Since these are velocity records we expect the spectra to increase with frequency over this frequency band. Instrument calibration is uncertain so units are not listed on the plot.

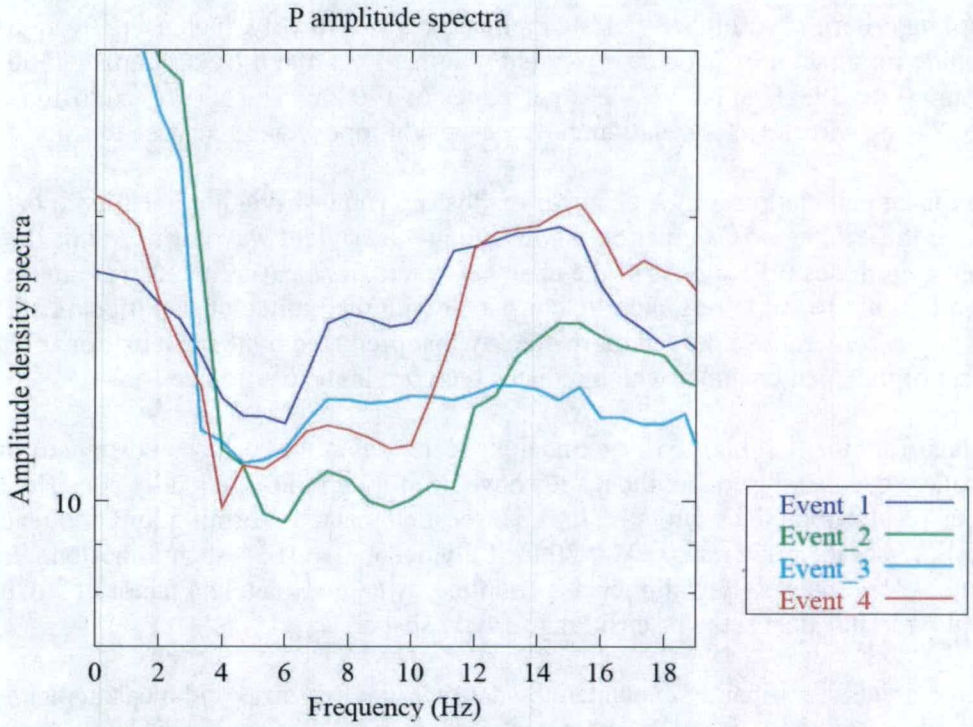

Figure 43. P-wave spectra from station 3 (11.4 km) of the four events. The GBV system response has been removed and replaced with the HFS response.

6 CONCLUSIONS AND RECOMMENDATIONS

We collected and analyzed data from 15 partially decoupled chemical explosions conducted in rectangular chambers at Älvdalen, Sweden. This data set covers a range of yields overdriven beyond full decoupling according to the Latter criterion by factors of up to 25. We find that chemical decoupling remains approximately complete for yields less than 10 times the Latter decoupling criterion. At higher yields coupling increases rapidly, increasing by an order of magnitude for a factor of 2 increase in yield/volume. Even the fully decoupled 2500 kg explosion is detectable at NORSAR at a distance of 140 km. The 500 kg explosion was also detected using waveform correlation, however waveforms were otherwise to small for analysis.

3D nonlinear calculations of the chamber explosions show strong nonlinearity at the points closest to the explosion. Calculations show stronger near field waveforms in this direction, with reduced amplitudes off the ends of the chamber where the measurements were made. Calculations are found to be generally consistent with the limited observational data set except that cavity reverberations die out more quickly that predicted by the calculations. This could be an effect of the open chamber which reduces pressure in the cavity over time.

New data from the Kirghizia Mine explosions recorded on the surface at distances of 5 km and 10 km have been analyzed and the results have been found to be generally consistent with previous results obtained from more limited free-field data, confirming low frequency chemical decoupling factors in the range of 20-30 for fully decoupled HE tests in limestone. Explosions detonated close to a cavity wall increase coupling by approximately a factor of 2. Chemical decoupling in this data set is insensitive to cavity shape.

This project has significantly expanded the data set of waveforms and measurements from decoupled and partially decoupled chemical explosions. Additional expansion is possible through recording and analysis of continuing explosions at Älvdalen, and frequent decoupled explosions at Løkken Gruver.

7 REFERENCES

Forsén, R., Hansson, H. and Carlberg, A. (1997), "Large Scale Test on Mitigation Effects of Water in the KLOTZ Club Installation in Älvdalen," Report FOA-R-97-00470-311 of the Swedish Defence Research Establishment (FOA), March.

Grønsten, G. A. (2000), "The Älvdalen Large Scale Tests", Data report from the Norwegian measurements, Fortifikatorisk notat nr. 286/01, Forsvarets Bygningstjeneste, Oslo, Norway, 2000.

Grønsten, G. A. and Krest, O. (2002), "The Älvdalen Large Scale Tests", Data report from the Norwegian measurements, Fortifikatorisk notat nr. 297/01, Forsvarets Bygningstjeneste, Oslo, Norway, 2001.

Hansson, H, and Forsén, R (1997), "Mitigation effects of water on ground shock: Large scale testing in Älvdalen," Report FOA-R-97-00510-311-SE of the Swedish Defence Research Establishment (FOA), May.

Herbst, R. F., G. C., Werth and D. L. Springer (1961), "Use of Large Cavities to Reduce Seismic Waves From Underground Explosions," J. Geophys. Res., 66, p. 959.

Kitov, I. O., D. D. Sultanov, V. V. Adushkin, V. N. Kostuchenko, O. P. Kuznetsov, P. B. Kaazik, N. I. Nedoshivin, H. D. Rubinshtein (1995), "Analysis of the Seismic Characteristics of U.S. and Russian Coupled and Cavity Decoupled Explosions in Salt," Institute for the Dynamics of the Geospheres, Final Report 911412, August.

Lee, E., M. Finger and W. Collins, (1973), "JWL equation of state coefficients for high explosives," Lawrence Livermore Laboratory UCID-16189, Jan, 16.

Murphy, J. R., I. O. Kitov, N. Rimer, V. V. Adushkin and B. W. Barker (1997), "Seismic Characteristics of Cavity Decoupled Explosions in Limestone: An Analysis of Soviet High Explosive Test Data," Journal of Geophysical Research, 102, B12, pp. 27, 393-27, 405.

Stevens, J. L., J. R. Murphy and N. Rimer (1991), "Seismic Source Characteristics of Cavity Decoupled Explosions in Salt and Tuff," Bull. Seism. Soc. Am., 81, pp. 1272-1291.

Stevens, J. L., N. Rimer, H. Xu, G. E. Baker and S. M. Day (2003), "Near field and regional modeling of explosions at the Degelen Test Site," SAIC final report to DTRA, SAIC-02/2050, January.

Stevens, Jeffry L., Norton Rimer, Heming Xu, G. Eli Baker, John R. Murphy, Brian W. Barker, Conrad Lindholm, Frode Ringdal, Steven Gibbons, Tormod Kvaerna and Ivan Kitov (2002), "Analysis and Simulation of Cavity-Decoupled Chemical Explosions," SAIC Annual Report No. 1 submitted to the Defense Threat Reduction Agency, SAIC-02/2046, October.

Thomson, D. J. (1982), "Spectrum estimation and harmonic analysis," Proc. IEEE, 70(9), 1055-1096.

Vretblad, B. (1991), "Klotz Club Tests 1986-1989, Report C1:91, Fortifikationsförvaltningen, Forskningsbyrån, Eskilstuna, Sweden.